We thank the two reviewers for their thoughtful comments. Our responses are in blue. Trackable changes relative to the last manuscript are also attached at the end.

**Anonymous Referee #1**
Received and published: 8 February 2020

In this paper, Zhu et al. evaluated OMI HCHO retrievals using in situ measurements from 12 airborne field campaigns (mostly over the U.S.) and the GEOS-Chem chemical transport model. They first compared GEOS-Chem simulated HCHO with aircraft measurements and used a constant scaling factor for each field campaign to correct the biases in GEOS-Chem simulations. The bias-corrected GEOS-Chem HCHO vertical column densities (VCDs) were then compared with OMI retrievals. It was found that OMI retrievals were generally biased high for low-HCHO conditions and had relatively small biases for high-HCHO cases. Potential reasons for the biases in OMI retrievals were also discussed. Overall, this is a useful study for understanding the quality and uncertainty in OMI HCHO retrievals. The authors expanded upon their previous study using the same approach (Zhu et al., 2016) to different locations and seasons. The advantage of the approach is that by using GEOS-Chem as a transfer standard, data from different field campaigns (often involving different instruments) can be used in a more consistent way for satellite validation. The paper is generally well written. There are, however, several points that need to be clarified. I would recommend that the paper be accepted for publication after the following comments have been addressed.

Specific Comments:
González Abad et al. (2015) showed that there were fairly large changes in OMI HCHO retrievals over remote background areas between the beginning of OMI (2004-2005) and more recent years (2012 and later). All the field campaigns discussed in this study took place after 2013. Have the authors looked into data from earlier field campaigns to check, for example, whether OMI retrieval biases under low-HCHO conditions were smaller in earlier years?

To our knowledge, there were only two flight campaigns, INTEX-B (2006) and MILAGRO (2006), before 2013 that reported in situ HCHO observations. Unfortunately, we failed to obtain INTEX-B HCHO data, and MILAGRO flight campaign is too localized over the Mexico City, so neither one was included in this validation study. The difference in HCHO retrievals over remote background regions between the beginning of OMI and more recent years is mainly due to the aging of the OMI instrument, which was further examined by analyzing the drift of HCHO columns over the remote Pacific [Zhu et al., 2014; 2017a]. OMI HCHO retrieval group at Harvard-SAO has been aware of the issue, and will fix it in the next version SAO HCHO product. We have added one sentence in the text to address the reviewer's concern, please see line 87-88.

Given the positive biases over low-HCHO areas and (smaller but mostly negative) biases over high HCHO areas in GEOS-Chem simulations, using a fixed scaling factor may not be appropriate for some of the field campaigns. For example, as shown in Figure 4, the mean HCHO VCD can range from ~ 3*10^15 molecules/cm^2 to over 10^16 molecules/cm^2 and it is possible that GEOS-Chem overestimates HCHO over relatively clean areas in the southwest corner of the

domain, and at the mean time underestimates HCHO over the southeast corner of the domain. Also by changing the domain slightly (for example, expand the domain to the west), the comparisons between OMI and bias-corrected GEOS-Chem can probably yield somewhat different results.

Accepted. We now limit the validation results (*e.g.*, in Table 2) only to the grids sampled by the aircraft (marked with open circles in Figure 4 and S1-S11).The manuscript is updated accordingly.

The authors proposed the validation method as a "global validation platform". Since the field campaigns discussed in this paper had no coverage outside of North America and Asia Pacific region, this is hardly "global".

Accepted. We have deleted the word "global".

Also for the method to be a "platform", there should be some utilities or applications that facilitate the validation of not just NASA OMI HCHO retrievals, but also retrievals from other satellite sensors/algorithms. Maybe there should also be functionality to ingest additional field campaign data and/or CTM simulations to be used in validation. I wonder if the authors can discuss these aspects of the validation platform (probably as an appendix).

Accepted. We now have added Appendix B to further discuss how to ingest additional field campaign and CTM data. Please see line 325-342.

Technical Comments:
Figure 3 is discussed quite extensively in two parts: lines 119-125 and lines 155-161.Maybe the authors can re-organize and consolidate the two parts?

We appreciate the reviewer's comment. We tried to change the text structure by re-organizing the two parts. However, we may want to stick to the current layout as it fits better to the logic flow: lines 119-125 (Section 2) are about the observed HCHO vertical profiles, while lines 155-161 (Section 3) are about GEOS-Chem modeled results. Figure 3 shows both observed and modeled HCHO vertical profiles, which is an essential part of this study, so that it may deserve in-depth discussion.

**Anonymous Referee #2**
Received and published: 10 February 2020

Zhu et al. present a new validation platform for satellite HCHO products, using different aircraft measurements and the model GEOS-Chem as the inter-comparison method. The model is used to make the link between the localised aircraft vertical measurements and the global satellite vertical columns. The method was introduced by Zhu et al. (2016). It is now extended to a larger number of aircraft campaigns, covering a broad range of conditions. An extensive evaluation of the NASA operational OMI HCHO satellite product is presented as an application of the platform. The retrieval steps of the satellite product are examined separately in order to explain the differences between satellite and aircraft results. The paper concludes with a slight bias of the OMI satellite product for high HCHO level, and to a high positive bias for low columns. This study addresses the need for more systematic validation of the satellite products. The use of several aircraft measurements combined with 3D-CTM is pretty new. It allows for direct and indirect validation of the vertical HCHO profiles, which is lacking in the community. A significant amount of work has been dedicated to this goal, and to present the results in an honest and clear way. However, the paper would benefit from some clarifications, especially at the end of the discussion. I recommend publication after the following points have been improved:

The authors claim for a global validation platform. This is supposed to be achieved through the model, but nothing is shown about this extension of the validation beyond the aircraft domains. Can the author add an illustration of this extension? A global map, or a comparison at another location? Alternatively, remain focused on the regions covered by the aircraft campaigns and leave out the reference to the global method.

Accepted. We have deleted the word “global”. We may want to point out that a global map is given in Figure 1 (panel a).

In the abstract, it is stated that the high biases are due to slant column fitting and radiance sector correction. It is not clearly demonstrated in the paper.

Accepted. We have rewritten this sentence in the abstract. Please see line 28-29.

The last paragraph of section 4 needs to be revised. The explanations are not clear, and conclusions are drawn without showing any results. It does not hold by itself, and needs to be extended (see my comments below).

Accepted. We have deleted and rewritten related sentences. Please see line 248-253.

The study look for systematic biases: Pay attention to data selection that can also introduce systematic bias (see my comments below).

Accepted. We now use new criteria (-0.8x$10^{16}$ molecules $cm^{-2}$ to 7.6x$10^{16}$ molecules $cm^{-2}$) to filter out the outliner, please see line 198-200. The manuscript is updated accordingly.

Does the biases found in this study match the error provided in the satellite product? What about precision? Does the validation results agree with provided satellite product precision?

We appreciate the reviewer's comment. Unfortunately, precision information is not provided in SAO product as reported by [González Abad et al. 2015]. We have added one sentence in the text to address the reviewer's concern. Please see line 198-200.

Introduction p3, line83: "global validation platform . . ... Using observations from 12 aircraft campaigns all over the world". I don't fully agree that this study is global. Results are shown only at the aircraft campaign locations. And those cover mostly US, Pacific and one over Korea. Important emission regions are missing all over the world. I would rather mention here the diversity of the seasonal coverage.

Accepted. We have deleted the word "global".

Application to NASA operational HCHO product Line 169: the so called "radiance reference sector correction term s0"is a slant column. Why do you use the term "radiance"? It is confusing. Does it refer to the reference spectra used during the DOAS fit? If yes, it should be better explained.

Accepted. We have replaced "radiance reference sector correction" with "reference sector correction" in the text.

Line 174: it is said that s0 is the difference between the retrieved SCD over the Pacific Ocean the GEOS-Chem climatology. Please explain if the model vertical columns are directly subtracted from the satellite slant columns (assumption AMF ~ ~ 1 over Pacific Ocean, which is not true), or if an air mass factor is used to convert the GEOS-Chem vertical columns into slant columns.

Accepted. We have rewritten this sentence to clarify. Please see line 177-178.

Line 194: selection criteria (4): VCD within the range -0.5x$10^{16}$ molecules $cm^{-2}$ to 1.0xe$10^{17}$ molecules $cm^{-2}$. Please provide the dispersion of the OMI HCHO VCD. If the VCD dispersion is, let's say, 0.8x1016 molecules cm-2, the lower limit might be too strict, removing a significant part of the distribution (negative columns) when the averaged column is close to zero, therefore biasing the averaged column to high values (case"high biases under low-HCHO conditions"). I suggest to test the impact on the comparisons if a more relaxed selection, based on a classical 3approach, is used.

Accepted. We now use new criteria (-0.8x$10^{16}$ molecules $cm^{-2}$ to 7.6x$10^{16}$ molecules $cm^{-2}$) to filter out the outliner, please see line 198-200. The manuscript is updated accordingly.

Line 207: Is the limit of 1.1 x $10^{16}$ for high-HCHO conditions based on satellite or model results? It looks like it is based on satellite columns, which is strange since it is the dataset to be validated, and it presents biases.

Accepted. The limit is based on satellite results. We have rewritten this sentence to clarify. Please see line 213-215.

Line 213: (2) please elaborate on the differences between the "radiance reference sector correction". Same for point (3) "selection criteria".

Accepted. We have removed point (2), and rewritten point (3). Please see line 221.

Line 223: Half of the bias in high-HCHO conditions can be attributed to a priori profiles but not the full bias. Please discuss other possible reasons for the remaining bias.

Accepted. We have rewritten related sentences to clarify. Please see line 225-235.

Line 229: Second case, low-HCHO conditions: I don't agree with the first conclusion. The a priori profiles are not the unique error source in the AMF calculation. It is not because the use of a more precise profile does not improve the comparison that the error is not due to AMF uncertainties. It could be due to albedo uncertainty; or imperfect cloud correction. However, I agree with the rest of the paragraph. Please reformulate the second line.

Accepted. We have rewritten this sentence to clarify. Please see line 237-238.

Line 240: "The SAO retrieval algorithm conducts the radiance reference sector correction by removing the contribution of HCHO over the remote Pacific Ocean to the radiance reference." What are the units of this contribution? A slant column or a radiance? Please explain what you mean by radiance reference. Line 241: Could you give a number for this HCHO contribution? Line 245: What do you mean by"suppressing removal of HCHO contribution in the radiance reference"? Line 246: "the mean bias is reduced from 147% to 128%". Where does this 128% come from? Furthermore, the bias reduction is not significant.

Accepted. We have removed this part to avoid ambiguity.

Line 248: "we attribute the remaining biases to (2) the latitudinal dependency of the radiance reference sector correction." Again this needs further explanations. Is there a latitudinal dependency of the slant columns, if yes positive or negative? And is there a latitudinal dependency in the current reference sector correction of the SAO product?

Accepted. We have removed this part to avoid ambiguity.

Line 249: You find a significant correlation of the satellite HCHO columns with the surface albedo during some campaigns, maybe even larger than the correlation with the model columns. It is interesting. Please specify for which campaigns?

Accepted. The campaigns are now listed in the text. Please see line 250.

If the reflectance climatology contains uncertainties, it will reflect in AMF uncertainties, that will not correct the slant columns for this kind of dependency. Therefore, it is important to know if AMF are used to compute s0. See my comment for line 174. Also, have you tested to remove sun glint scenes from the comparison for the Pacific regions?

Accepted. We have rewritten this sentence to clarify, please see line 177-178. Based on our understanding, sun-glint scenes were already removed in the retrieval process sing the sun-glint warning flag.

Figure 4 and supplement: spatial correlation between model and satellite column seems rather low. Please add correlations in Table 2.

Accepted. Spatial correlations between model and satellite columns are now given in Table 2.

Why not using the same scale for OMI and the model? for example from 0 to $20x10^{15}$ molecules $cm^{-2}$? As it is now, it seems badly chosen for OMI.

Accepted. We now use the same scale for OMI and modeled columns.

# Validation of satellite formaldehyde (HCHO) retrievals using observations from 12 aircraft campaigns

Lei Zhu[1,2], Gonzalo González Abad[1], Caroline R. Nowlan[1], Christopher Chan Miller[1], Kelly Chance[1], Eric C. Apel[3], Joshua P. DiGangi[4], Alan Fried[5], Thomas F. Hanisco[6], Rebecca S. Hornbrook[3], Lu Hu[7], Jennifer Kaiser[8,9], Frank N. Keutsch[10,11,12], Wade Permar[7], Jason M. St. Clair[6,13], Glenn M. Wolfe[6,13]

[1]Harvard-Smithsonian Center for Astrophysics, Cambridge, MA, USA
[2]School of Environmental Science and Engineering, Southern University of Science and Technology, Shenzhen, China
[3]Atmospheric Chemistry Observations & Modeling Laboratory, National Center for Atmospheric Research, Boulder, CO, USA
[4]NASA Langley Research Center, Hampton, VA, USA
[5]Institute of Arctic & Alpine Research, University of Colorado, Boulder, CO, USA
[6]Atmospheric Chemistry and Dynamic Laboratory, NASA Goddard Space Flight Center, Greenbelt, MD, USA
[7]Department of Chemistry and Biochemistry, University of Montana, Missoula, MT, USA
[8]School of Civil and Environmental Engineering or Earth, Georgia Institute of Technology, Atlanta, GA, USA
[9]School of Earth and Atmospheric Sciences, Georgia Institute of Technology, Atlanta, GA, USA
[10]John A. Paulson School of Engineering and Applied Sciences, Harvard University, Cambridge, MA 02138, USA
[11]Department of Chemistry and Chemical Biology, Harvard University, Cambridge, MA 02138, USA
[12]Department of Earth and Planetary Sciences, Harvard University, Cambridge, MA 02138, USA
[13]Joint Center for Earth Systems Technology, University of Maryland Baltimore County, Baltimore, MD, 21228, USA

*Correspondence to*: Lei Zhu (~~lei.zhu.02@gmail.com~~zhul3@sustech.edu.cn)

**Abstract.** Formaldehyde (HCHO) has been measured from space for more than two decades. Owing to its short atmospheric lifetime, satellite HCHO data are used widely as a proxy of volatile organic compounds (VOCs; please refer to Appendix A for abbreviations and acronyms), providing constraints on underlying emissions and chemistry. However, satellite HCHO products from different satellite sensors using different algorithms have received little validation so far. The accuracy and consistency of HCHO retrievals remain largely unclear. Here we develop a ~~global~~ validation platform for satellite HCHO retrievals using *in situ* observations from 12 aircraft campaigns with a chemical transport model (GEOS-Chem) as the intercomparison method. Application to the NASA operational OMI HCHO product indicates ~~slight~~ negative biases (~~–30.9~~–44.5% to ~~+16.0~~–21.7%) under high-HCHO ~~conditions partially caused by *a priori* shape factors used in the retrievals,~~ condition while high biases (~~+13.9~~66.1% to ~~+194.6~~112.1%) under low-HCHO ~~conditions due mainly to slant column fitting and radiance reference sector correction~~conditions. Under both conditions, HCHO *a priori* vertical profiles are likely not the main driver of the biases. By providing quick assessment to systematic biases in satellite products over large domains, the platform facilitates, in an iterative process, optimization of retrieval settings and the minimization of retrieval biases. It is also complementary to localized validation efforts based on ground observations and aircraft spirals.

## 1 Introduction

Formaldehyde (HCHO) is ubiquitous in the troposphere due to its high product yields from atmospheric oxidation of volatile organic compounds (VOCs). Methane mainly controls the tropospheric background, whereas regional enhancements are contributed largely by short-lived non-methane VOCs (NMVOCs) emitted from the biosphere, human activities, and wildfires. HCHO is detectable from space using solar ultraviolet backscattered radiation between 325 and 360 nm [Chance et al., 2000]. HCHO vertical column densities (VCDs; in the unit of molecules $cm^{-2}$) are obtained after the retrieval process and the consideration of *a priori* information. Because of the short atmospheric lifetime of HCHO (a few hours), satellite HCHO VCD has been used as a localized proxy for NMVOC emissions [*e.g.*, Palmer et al., 2003; Shim et al., 2005; Stavrakou et al., 2009; Marais et al., 2012; Barkley et al., 2013; Zhu et al., 2014; Zhu et al., 2017a; Cao et al., 2018; Surl et al., 2018]. In addition, previous applications of HCHO retrievals also include evaluating surface ozone sensitivity [Jin and Holloway, 2015; Jin et al., 2017], quantifying cancer risks of ambient HCHO [Zhu et al., 2017b], estimating organic aerosol abundance [Liao et al., 2019], and mapping hydroxyl (OH) radicals [Wolfe et al., 2019]. However, validation of satellite HCHO products from different satellite sensors using different algorithms have received little attention so far. Validation exercises over different regions in different seasons remain extremely limited. Here we develop a validation platform built with HCHO observations from 12 aircraft campaigns over the United States, Eastern Asia, and the remote Pacific Ocean. We further apply it to the NASA operational HCHO product and report the validation results.

HCHO has been continuously observed from space for more than two decades since GOME (1996–2003) [Chance et al., 2000; De Smedt et al., 2008] and SCIAMACHY (2003–2012) [Wittrock et al., 2006; De Smedt et al., 2008]. Presently available observations are from OMI (2004–) [De Smedt et al., 2015; González Abad et al., 2015], GOME-2A (2006–) [De Smedt et al., 2012], OMPS (2011–) [Li et al., 2015; González Abad et al., 2016], GOME-2B (2012–) [De Smedt et al., 2012], and TROPOMI (2018–) [De Smedt et al., 2018]. Hourly HCHO observations (in daytime) will be made available from a constellation of geostationary satellites to be launched in the coming 1–3 years, including GEMS (2020) [Kim et al., 2019; Kwon et al., 2019] over Eastern Asia, TEMPO (2022) [Zoogman et al., 2017] over North America, and Sentinel-4 (2023) [Courrèges-Lacoste et al., 2017] over Europe. HCHO retrieved from the above satellites generally follows a two-step approach, slant column density (SCD) fitting and conversion of it to VCD using localized air mass factors (AMFs), with retrieval errors being introduced in each step [Marais et al., 2012; De Smedt et al., 2015; González Abad et al., 2015; Hewson et al., 2015; Kwon et al., 2017; Herman et al., 2018; Nowlan et al., 2018].

Previous validation of HCHO satellite data sets is often conducted by directly comparing coincident satellite pixels and observation points. Wittrock et al. [2006] and Vigouroux et al. [2009] found SCIAMACHY HCHO columns are unbiased compared with ground-based measurements over remote regions. De Smedt et al. [2015] reported OMI and GOME2 data are –20% to –40% biased against observed vertical profiles. Wang et al. [2017] reported biases in OMI and GOME2 data

of –12% to –20% over the Eastern China from May to December. A recent study showed monthly bias in OMI data ranges from –11% in summer to +26% in winter in Beijing between 2010 and 2016 [Wang et al., 2019]. Comparison with aircraft observations indicated that GOME data are +16% biased during summer over Eastern Texas in the United States [Martin et al., 2004], and that OMI data are biased by –37% in October over Guyana [Barkley et al., 2013]. Tan et al. [2018] found OMPS data are –18% biased against ship-based measurements in June over the East China Sea.

Such direct validation approaches, however, face three practical challenges. First, they require the averaging of extensive observations to reduce large random noises associated with individual satellite retrievals. Second, they fail to make full use of precise *in situ* observations. Low earth orbit (LEO) satellites pass over a certain location within a fixed time window up to a couple of times per day, meaning only a small fraction of observations are coincident with satellite pixels thus suitable for the purpose of direct validation. Finally, reliability of validation results is unclear for areas beyond the observation sites/domains.

Alternatively, Zhu et al. [2016] proposed an indirect validation approach with a chemical transport model (CTM) as the intercomparison method. This approach increases considerably the range of data and conditions that can be used for validation, and therefore reduces random noises in satellite retrievals through averaging. Using this approach, Zhu et al. [2016] found current HCHO satellite products are biased by –20% to –51% against the SEAC$^4$RS [Toon et al., 2016] aircraft measurements over the Southeastern United States during the summer of 2013. Here we follow this indirect validation approach to develop a ~~global~~ validation platform for satellite HCHO retrievals using observations from 12 aircraft campaigns all over the world, as discussed below.

## 2 HCHO observations from aircraft campaigns

Figure 1 shows flight tracks of 12 aircraft campaigns used in this study. Detailed information is summarized in Table 1. The 12 aircraft campaigns are selected based on the data availability and spatial representativeness. Together, the 12 aircraft campaigns offer exceptional opportunities for ~~global~~ validating of satellite HCHO retrievals with extensive observations over the United States (C1–C9; DISCOVER-AQ California 2013, NOMADSS, SENEX, DISCOVER-AQ Texas 2013, DISCOVER-AQ Colorado 2014, FRAPPÉ, WINTER, SONGNEX, and WE-CAN, respectively), Eastern Asia (C10; KORUS-AQ), and the remote Pacific Ocean (C11–C12; ATom-1 and ATom-2). The aircraft campaigns have great spatial coverages over HCHO hotspots, such as the Southeastern United States (C2 and C3) dominated by strong biogenic isoprene emissions [Guenther et al., 2012], Houston area (C4) featured with high anthropogenic NMVOCs [Zhu et al., 2014], and the Western United States (C9) influenced by wildfires. The campaigns also survey different seasons of the year, enabling assessment of seasonal biases in satellite HCHO products.

During the aircraft campaigns, HCHO observations were made along the flight tracks with multiple instruments, including (1) NCAR Difference Frequency Generation Absorption Spectrometer (DFGAS) [Weibring et al., 2006, 2007, 2010], (2) Trace Organic Gas Analyzer (TOGA) [Apel et al., 2003; 2010; 2015], (3) In Situ Airborne Formaldehyde instrument (ISAF) [Cazorla et al., 2015], (4) Compact Atmospheric Multispecies Spectrometer (CAMS) [Fried et al., 2011; Richter et al., 2015], and (5) Proton Transfer Reaction Time-of-Flight Mass Spectrometer (PTR-ToF-MS) [Müller et al., 2014]. The instrument accuracy ($1\sigma$ level) is 4.5%, 15% (lower limit; https://airbornescience.nasa.gov/instrument/TOGA), 10% [Cazorla et al., 2015], 4% [Richter et al., 2015], and 60% [Hu and Permar, 2019] for DFGAS, TOGA, ISAF, CAMS, and PTR-ToF-MS, respectively. The corresponding instrument detection limits are 40–100 ppt [Nowlan et al., 2018], 20 ppt [Wofsy et al., 2018], 36 ppt [Cazorla et al., 2015], ~ 40 ppt [Richter et al., 2015] and 300 ppt [Hu and Permar, 2019], respectively.

HCHO observations from different instruments are generally consistent. Zhu et al. [2016] reported ISAF to be in good agreement with CAMS during the SEAC$^4$RS campaign with a correlation coefficient ($r$) of 0.99 and a slope of 1.10. ISAF is also found consistent ($r$=0.98) with DFGAS during the DC3 campaign [Barth et al., 2015] with a slope of 1.07 [Liao et al., 2019]. Figure 2 shows point-to-point comparisons among 1-min averaged TOGA, ISAF, and CAMS HCHO observations aboard the aircrafts. There is a high correlation in the mixed layer (here and elsewhere defined as below 2 km; $r$=0.86) and free troposphere (> 2 km; $r$=0.93) between TOGA and CAMS during the FRAPPÉ campaign with a Reduced major axis (RMA) regression slope of 1.05±0.01. During the WINTER campaign, TOGA generally matches with ISAF ($r$=0.72) within the mixed layer. However, consistency between the two instruments begins to fall apart in the free troposphere ($r$=0.33), which is likely driven by sampling differences. TOGA correlates highly with ISAF during the ATom-2 (C12) campaign in both mixed layer ($r$=0.83) and free troposphere ($r$=0.82), but overall it is 48% higher than ISAF likely due to the fact that the two instruments are independently calibrated. In this study, we use CAMS data for FRAPPÉ (C6), ISAF data for both WINTER (C7) and ATom-2 (C12), given their higher accuracies.

Figure 3 shows mean vertical profiles measured from the 12 aircraft campaigns. For campaigns conducted over/near land (C1–C10), aircraft observations show higher level of HCHO within the mixed layer as a result of biogenic and anthropogenic NMVOC emissions. In the free troposphere, HCHO starts to drop sharply due to short lifetimes of highly reactive NMVOCs, such as isoprene (~ 1 h) and HCHO itself (~ 2 h). We see enhanced HCHO (~~2~~ > 3 ppb) in 43–5 km during the WE-CAN (C9) campaign, which is caused by intensive primary and secondary production of HCHO from wildfires in the Western United States. Mean HCHO over the remote Pacific Ocean (C11–C12) declines with altitudes through the troposphere (below 12 km), suggesting oxidation of well-mixed methane as the dominant source of the tropospheric background HCHO.

## 3 GEOS-Chem as the intercomparison method

The indirect validation approach requires a CTM to bridge sampling gaps between aircraft observations and satellite retrievals [Zhu et al., 2016]. Here we use GEOS-Chem version 12.0.0 (doi:10.5281/zenodo.1343547) as the intercomparison method for validation of satellite HCHO columns using aircraft observations. With a detailed representation of ozone-$NO_x$-VOCs-aerosol-halogens tropospheric chemistry, the GEOS-Chem model has been used extensively in several studies to simulate HCHO including comparisons with *in situ* observations [Jaeglé et al., 2015; Zhu et al., 2016; Chan Miller et al., 2017; Liao et al., 2019]. Zhu et al. [2016] and Chan Miller et al. [2017] found that GEOS-Chem provides an unbiased simulation of SEAC$^4$RS and SENEX aircraft observations within the mixed layer over the Southeastern United States in summer, including horizontal patterns and mean vertical profiles. In winter, GEOS-Chem is biased by −32% compared against aircraft observations below 300 m over the Northeastern United States [Jaeglé et al., 2015].

The GEOS-Chem model is driven by the Goddard Earth Observing System–Forward Processing (GEOS-FP) assimilated meteorological data, produced by the NASA Global Modeling and Assimilation Office (GMAO) [Molod et al., 2012]. The GEOS-FP meteorological data have a native horizontal resolution of 0.25°×0.3125° with 72 vertical pressure levels and 3 h temporal frequency (1 h for surface variables and mixed layer depths). Biogenic VOC emissions are from the MEGAN 2.1 model [Guenther et al., 2012] as implemented in GEOS-Chem by Hu et al. [2015]. Anthropogenic emissions are based on the NEI2011 inventory [EPA, 2015] over the United States, and the MIX inventory [Li et al., 2017] over the Eastern Asia region. Fire emissions are from the fourth-generation global fire emissions database (GFED4) [Giglio et al., 2013]. Surface-driven vertical mixing up to the mixing depth is based on the non-local mixing scheme of Holtslag and Boville [1993], as implemented in GEOS-Chem by Lin and McElroy [2010].

We run the GEOS-Chem model at a 2°×2.5° resolution to simulate the ATom-1 (C11) and ATom-2 (C12) campaigns as HCHO over the remote Pacific Ocean is relatively homogeneously distributed due to methane oxidation. Over the continents, we use the native resolution (0.25°×0.3125°, nested version) in GEOS-Chem to better represent heterogeneities in emissions and chemistry during the aircraft campaigns (C1–C10) over North America (130°–60°W, 9.75°–60°N) and Eastern Asia (70°–140°E, 15°–55°N). Dynamic boundary conditions for the nested simulations are from global 2°×2.5° runs. Global and nested simulations are spun up for 10 and 1 month, respectively, to remove the sensitivity to initial conditions. GEOS-Chem is sampled along the flight tracks at the time and locations of the aircraft measurements.

Figure 3 shows GEOS-Chem mean HCHO profiles. Previous studies [Scarino et al., 2014; Millet et al., 2015; Zhu et al., 2016] found GEOS-FP mixing depth in summer is biased low comparing with observations by a factor of 30%–50%, which may partially contribute to the underestimation of HCHO in the mixed layer (Figure 3) by GEOS-Chem over the Unites States (C1–C6, C9) and South Korea (C10). On top of that, underestimation of highly reactive VOC emissions as reported by

Zhu et al. [2014] may be another reason for the lower simulated HCHO over Houston area (C4). GEOS-Chem generally reproduces the observed vertical distribution of HCHO in the free troposphere. Exceptions are for campaigns surveying the Western United States in summer (C5, C6, and C9), likely caused by uncertainties in GFED4 fire emissions in the model.

By integrating the mean vertical profiles in Figure 3, we estimate, for each aircraft campaign, a mean observed HCHO column, a mean GEOS-Chem modeled HCHO column, and the regional bias associated with GEOS-Chem model as informed by comparison between observed and modelled HCHO columns. Figure 3 shows the regional bias for each aircraft campaign, which is later applied as the correction factor in the validation exercises.

## 4 Application to NASA operational HCHO product

NASA operational OMI HCHO product is based on the Smithsonian Astrophysical Observatory (SAO) HCHO retrieval algorithm [González Abad et al., 2015]. Briefly, the algorithm follows a two-step approach. First, a ~~radiance~~ reference sector correction term ($\Omega_{S0}$) is subtracted from the fitted total SCD ($\Omega_S$), yielding the ~~radiance~~ reference sector corrected SCD ($\Delta\Omega_S$):

$$\Delta\Omega_S = \Omega_S - \Omega_{S0} \quad (1)$$

Following Khokhar et al. (2005) and De Smedt et al. (2008), the ~~radiance~~ reference sector correction ($\Omega_{S0}$) represents a daily post-processing normalization for the retrieved SCD, calculated as the difference between the retrieved SCD over the Pacific Ocean and the GEOS-Chem ~~climatology~~ VCD climatology over the Pacific Ocean multiplied by satellite air mass factor (*AMF*) (González Abad et al., 2015; González Abad et al., 2016). $\Delta\Omega_S$ is then converted to VCD ($\Omega$) by applying ~~the localized air mass factor (~~corresponding *AMF*~~)~~:

$$\Omega = \frac{\Delta\Omega_S}{AMF} \quad (2)$$

The *AMF* depends on a number of factors, including solar zenith angle ($\theta_Z$), satellite viewing angle ($\theta_V$), cloud characteristics, scattering properties of the atmosphere and surface, and HCHO *a priori* profiles. Following Palmer et al. [2001], it is computed as the product of a geometrical *AMF* ($AMF_G$) and a correction with scattering weights *w* applied to the vertical shape factors *S*:

$$AMF = AMF_G \int_{P_S}^{0} w(p)S(p)dp \quad (3)$$

$$AMF_G = \sec\theta_Z + \sec\theta_V \quad (4)$$

Here the integration is over the pressure ($p$) coordinate from the surface ($P_S$) to the top of atmosphere. *S* is the normalized vertical profile of HCHO mixing ratios *C(p)*:

$$S(p) = \frac{C(p)\Omega_A(p)}{\int_{P_S}^{0} C(p)\Omega_A(p)dp} \quad (5)$$

where $\Omega_A(p)$ is the partial air column density at $p$, and $w$ measure the sensitivity of the backscattered radiation to HCHO. OMI SAO HCHO product provides $\Omega$, $\Omega_S$, $\Delta\Omega_S$, $AMF_G$ (in term of $\theta_Z$ and $\theta_V$), $AMF$, $S$, and $w$ for each pixel. Uncertainties associated with $\Omega$ are ~~45–105~~30%–100%, contributed by uncertainties in both $AMF$ (~ 35%) and $\Delta\Omega_S$ (30–100%) [González Abad et al. 2015].

Here we use the DISCOVER-AQ 2013 (C1) flight campaign as an example to demonstrate the validation process. Validation of OMI SAO HCHO product starts with the selection of satellite pixels. This is done for each campaign within the corresponding study period (Table 1) and domain (defined in Table 1; shown in Figure 1) based on following criteria: (1) pass quality checks (MainDataQualityFlag=0), (2) have cloud fraction less than 0.3, (3) have $\theta_Z$ less than 60°, and (4) have VCD within the range of ~~$-0.5\times10^{16}$~~ $8.0\times10^{15}$ molecules cm$^{-2}$ to ~~$1.0\times10^{17}$~~ $7.6\times10^{16}$ molecules cm$^{-2}$. The last criterion is set based on 3 times of the fitting uncertainty (30%–100%) and a typical VCD value between $4.0\times10^{15}$ molecules cm$^{-2}$ and $4\times10^{16}$ molecules cm$^{-2}$ [González Abad et al. 2015]. We then compute campaign-averaged GEOS-Chem HCHO columns by sampling the model according to OMI's schedule. The original GEOS-Chem columns are further scaled using correction factors informed by comparison of model and aircraft columns (Figure 3). Figure 4 shows campaign-averaged HCHO columns for both OMI SAO and corrected GEOS-Chem over the study domain (California, United States). Campaign-averaged OMI and corrected GEOS-Chem HCHO columns for other campaigns (C2–C12) are in the Supplement. Poor spatial correlations between OMI and corrected GEOS-Chem columns during some campaigns (Figure 4 and Supplement) likely reflect large uncertainties in OMI columns. Finally, we compare spatially and temporally averaged HCHO columns, during the study period and over the study domain, as reported by OMI SAO product and modelled by GEOS-Chem (with correction) to estimate the regional systematic bias in OMI SAO HCHO product. Detailed validation results are summarized in Table 2.

We see from Table 2 that relative biases in OMI HCHO product depends on both locations and seasons, ranging from ~~–30.9~~44.5% ~~over South Korea~~ in summer (~~C10~~C9) to ~~+194.6~~112.1% ~~over Western United States~~ in spring (C8) both over the Western United States. Overall, the relative biases in OMI SAO product fall into two categories. First, the product is ~~slightly~~ negatively biased (~~–30.9~~44.5% to ~~+16.0~~–21.7%) under high-HCHO conditions (arbitrarily defined as mean HCHO column > 1.~~00~~$\times10^{16}$ molecules cm$^{-2}$), such as summertime Southeastern ~~United States~~ (C2, C3, C4) and Western (C9) ~~and~~ United States as well as summertime South Korea (C10). A similar bias (–37.0%) in OMI SAO HCHO product is reported by Zhu et al. [2016] for summertime Southeastern United States. Second, the product is highly biased (+~~113.9~~66.1% to +~~194.6~~112.1%) under low-HCHO conditions, such as the Western United States (C5, C6, and C8), wintertime United States (C1 and C7), and the remote Pacific Ocean (C11 and C12). Our work points to a higher bias (~ ~~120~~70%) in OMI SAO retrievals over the remote Pacific Ocean compared with the bias (~ 10%) reported by Wolfe et al. [2019]. This is likely driven by a number of factors: (1) Wolfe et al. [2019] use all data, whereas we only use data over the Pacific region (Figure

1); (2) ~~radiance reference sector correction is treated differently in the two studies; (3~~selection criteria (e.g., $\theta_z$ and data filtering) ~~selection criteria~~ for OMI pixels are different; (~~4~~3) mean observed HCHO column is computed from individual profiles in Wolfe et al. [2019], while it is computed based on a mean profile in this study; (~~5~~4) and finally, the relative bias metric is more sensitive to absolute bias under low-HCHO conditions.

~~We attribute biases in the first case partially to~~ In both cases, *a priori* vertical profiles used in the SAO HCHO retrieval algorithm~~, in particular underestimate~~ are likely not the main drivers of ~~HCHO in~~ the ~~mixed layer~~biases. SAO HCHO algorithm samples HCHO shape factors (*S*) from a monthly mean climatology based on GEOS-Chem simulations in 2007 at a spatial resolution of 2°×2.5°, which may not be able to represent the spatial heterogeneity in chemistry, nor/or to model temporal variations in emissions. ~~After~~ In the first case, after recomputing the AMF with observed HCHO shape factors following equation (3)–(5)~~,~~ , relative biases in HCHO ~~can be reduced~~ reduce slightly on average from ~~–15.9~~36.5% to ~~–8.4~~32.6% (C3, C4, C9, and C10 in Table 2)~~. As shown in Figure 5~~. The largest improvement is seen for C3 and C4, where relative biases are reduced on average from –35.4% to –27.4%, because using observed HCHO shape ~~factors (C3, C4, and C9)~~ factors results in lower AMF by correcting underestimated *a priori* HCHO within the mixed layer (Figure 5). During the WE-CAN campaign (C9), recomputed AMF is slightly higher than that reported by OMI (Table 2) because of elevated HCHO around 3–5 km from wildfire plumes (Figure 5). In the second case, using observed HCHO shape factors, however, barely reduces biases in OMI SAO HCHO product (Table 2).

~~In the second case, using observed HCHO shape factors, however, barely reduces biases in OMI SAO HCHO product (Table 2), implying that radiance reference~~ Reference sector corrected SCD ($\Delta\Omega_S = \Omega_S - \Omega_{S0}$) ~~rather than~~ and/or other AMF ~~is~~ components (such as surface reflectivity and cloud correction) are likely the main ~~driver~~ drivers of high biases. This can be further examined with aircraft observations and OMI HCHO pixels over remote Pacific Ocean (C11 and C12), where contribution of $\Omega_{S0}$ to $\Delta\Omega_S$ is much lower (~ ~~15~~18%; Table 2). Integration of ATom1 (C11) and ATom2 (C12) vertical profiles indicates a Pacific background HCHO VCD of ~ $3.0\times10^{15}$ molecules $cm^{-2}$ (Figure 3), comparable with previous measured values ($2.8\times10^{15}$ molecules $cm^{-2}$ to $4.6\times10^{15}$ molecules $cm^{-2}$) over the remote North Pacific Ocean [Singh et al., 2009] and modeled results ($4.5\times10^{15}$ molecules $cm^{-2}$) [Wolfe et al., 2019]. This is equivalent to a background SCD of ~ $4.7\times10^{15}$ molecules $cm^{-2}$ with AMF computed using observed HCHO shape factors (Figure 5). OMI SAO SCD ($\Omega_S$) and ~~radiance~~ reference sector corrected SCD ($\Delta\Omega_S$) is much higher than such estimated background SCD value by a factor of ~ 2.0 ~~to 2.5~~ (Table 2), pointing to potential issues with SCD fitting and/or ~~radiance~~ reference sector correction in the SAO HCHO retrieval algorithm.

~~The SAO retrieval algorithm conducts the radiance reference sector correction by removing the contribution of HCHO over the remote Pacific Ocean to the radiance reference. This HCHO contribution is derived using a high-resolution solar~~

~~spectrum [Chance et al., 2010] convolved with the instrument response function. Despite OMI's stability over the mission lifetime [Schenkeveld et al., 2017], small spectral changes could have significant impacts on the derived HCHO columns over the remote Pacific Ocean where HCHO signals are relatively weak.~~ We ~~revaluate such impacts by supressing removal of HCHO contribution in the radiance reference. The new approach improves both spectral fitting results and retrieval stability during the life span of OMI. In consequence, mean bias in the resulted columns is reduced from 147.1% (Table 2) to 128.2% in the second case. We~~ attribute the remaining biases to ~~(1)~~ increased impact of interferers (*e.g.*, $O_3$ and BrO, $O_2$-$O_2$ and water vapor) when HCHO signals are ~~weak and (2) the latitudinal dependency of the radiance reference sector correction~~weak. We also find that OMI SAO HCHO VCD correlates moderately ($r$=0.38 to 0.66) with surface albedo during some campaigns (*i.e.*, C1, C5, and C6), suggesting possible bias introduced by using a reflectance climatology [Kleipool et al., 2008] in the retrievals. In summary, high biases under low-HCHO conditions are likely driven by both ~~radiance~~ reference sector correction and SCD fitting. An updated SAO product is being developed to minimize the biases by optimizing the two processes accordingly.

## 5 Conclusions

We have used HCHO observations from 12 aircraft campaigns, together with the GEOS-Chem chemical transport model as an intercomparison method, to develop a ~~global~~ validation platform for satellite HCHO retrievals. The ~~global~~ validation platform offers an alternative way to quickly assess systematic biases in satellite products over large spatial domains and longer temporal periods, facilitating optimization of retrieval settings and the minimization of retrieval biases. Application to NASA operational HCHO product (SAO retrievals) indicates that relative biases range from ~~–30.9~~44.5% to ~~+194.6~~112.1% depending on locations and seasons~~. Under~~. The product is negatively biased (–44.5% to –21.7%) under high-HCHO conditions, such as summertime Southeastern United States,, ~~the product is slightly~~ while positively biased (~~–30.9~~+66.1% to ~~+16.0~~112.1%) ~~due partially to underestimate of HCHO within the mixed layer by *a priori* profiles. Under~~ under low-HCHO conditions, such as wintertime United States and remote Pacific Ocean. Under both conditions, HCHO *a priori* vertical profiles are likely not the ~~product is highly biased (+113.9% to +194.6%), likely as a result of slant column density fitting process of HCHO.~~ main driver of the biases. Our work points to the need for improvement in OMI SAO HCHO product to correct the systematic biases, particularly, optimization of the HCHO slant column fitting and reference sector correction.

## Data and code availability

The validation platform (R scripts) is available at: https://doi.org/10.7910/DVN/KG3XNC.

The GEOS-Chem model is available at http://acmg.seas.harvard.edu/geos/ (last access: Nov. 29, 2019).

OMI-SAO HCHO data were downloaded from http://disc.sci.gsfc.nasa.gov/Aura/dataholdings/OMI/omhcho_v003.shtml.

Aircraft observations are available respectively as following:

DISCOVER-AQ California 2013 (C1): https://www-air.larc.nasa.gov/missions/discover-aq/discover-aq.html

NOMADSS (C2): https://www.eol.ucar.edu/field_projects/nomadss/

SENEX (C3): https://www.esrl.noaa.gov/csd/projects/senex/

DISCOVER-AQ Texas 2013 (C4): https://www-air.larc.nasa.gov/missions/discover-aq/discover-aq.html

DISCOVER-AQ Colorado 2014 (C5): https://www-air.larc.nasa.gov/missions/discover-aq/discover-aq.html

FRAPPÉ (C6): http://catalog.eol.ucar.edu/FRAPPE/

WINTER (C7): http://catalog.eol.ucar.edu/winter/

SONGNEX (C8): https://www.esrl.noaa.gov/csd/projects/songnex/

WE-CAN (C9): https://www.eol.ucar.edu/field_projects/we-can/

KORUS-AQ (C10): https://www-air.larc.nasa.gov/missions/korus-aq/

ATom-1 (C11): https://daac.ornl.gov/ATOM/campaign/

ATom-2 (C12): https://daac.ornl.gov/ATOM/campaign/

## Appendix A

*Abbreviations and acronyms*

| | |
|---|---|
| AMF | Air mass factor |
| $AMF_G$ | Geometrical Air mass factor |
| ATom | Atmospheric Tomography Mission |
| CAMS | Compact Atmospheric Multispecies Spectrometer |
| CTM | Chemical transport model |
| DC3 | Deep Convective Clouds and Chemistry Experiment |
| DFGAS | Difference Frequency Generation Absorption Spectrometer |
| DISCOVER-AQ | Deriving Information on Surface Conditions from COlumn and VERtically Resolved Observations Relevant to Air Quality |
| FRAPPÉ | Front Range Air Pollution and Photochemistry Éxperiment |
| GEMS | Geostationary Environment Monitoring Spectrometer |
| GEOS-FP | Goddard Earth Observing System–Forward Processing |
| GFED4 | Fourth-generation Global Fire Emissions Database |
| GMAO | Global Modeling and Assimilation Office |
| GOME(-2) | Global Ozone Monitoring Experiment(-2) |
| HCHO | Formaldehyde |
| ISAF | In Situ Airborne Formaldehyde |
| KORUS-AQ | Korea-United States Air Quality |

| | |
|---|---|
| LEO | Low Earth Orbit |
| MEGAN | Model of Emissions of Gases and Aerosols from Nature |
| NEI | National Emissions Inventory |
| NMVOCs | Non-Methane VOCs |
| NOMADSS | Nitrogen, Oxidants, Mercury, and Aerosol Distributions, Sources, and Sinks |
| OMI | Ozone Monitoring Instrument |
| OMPS | Ozone Mapping and Profiler Suite |
| PTR-ToF-MS | Proton-Transfer-Reaction Time-of-Flight Mass Spectrometer |
| RMA | Reduced major axis |
| SAO | (Harvard) Smithsonian Astrophysical Observatory |
| SCD | Slant Column Density |
| SCIAMACHY | Scanning Imaging Absorption spectroMeter for Atmospheric Chartography |
| SEAC$^4$RS | Studies of Emissions, Atmospheric Composition, Clouds and Climate Coupling by Regional Surveys |
| SENEX | Southeast Nexus |
| SONGNEX | Shale Oil and Natural Gas Nexus |
| TEMPO | Tropospheric Emissions: Monitoring of Pollution |
| TOGA | Trace Organic Gas Analyzer |
| TROPOMI | TROPOspheric Monitoring Instrument |
| VCD | Vertical Column Density |
| VOCs | Volatile Organic Compounds |
| WE-CAN | Western wildfire Experiment for Cloud chemistry, Aerosol absorption and Nitrogen |
| WINTER | The Wintertime INvestigation of Transport, Emissions, and Reactivity |

## Appendix B

*Validation platform*

1. Source code

The validation platform (R scripts) is available at: https://doi.org/10.7910/DVN/KG3XNC.

Please download all the files, and follow the instructions in NOTE to install required R packages and run the script.

Sample scripts for processing aircraft, CTM, and satellite data are available at: https://www.acmrsg.org/datasets.

Please use process.R and compute.R for step 2-5.

2. Ingesting additional field campaign data

To process additional field campaign data, a user needs to sample the CTM along the flight tracks. This can be done with GEOS-Chem flight diagnostic (http://wiki.seas.harvard.edu/geos-chem/index.php/Planeflight_diagnostic). Please follow

process.R (line 117-381) for processing GEOS-Chem flight diagnostic output files. For other CTMs, similar functionality may need to be developed/used.

3. Preparing CTM data

A user also needs to prepare CTM according to satellite schedules. Please follow process.R (line 384-593) for more.

4. Processing new HCHO retrievals

To validate new HCHO retrievals, a user needs to read, clean, filter, and regrid level 2 satellite data. Please follow process.R (line 595-884) for more.

5. Validation of new HCHO retrievals

Finally, we have a sample script (compute.R) for computing and plotting the validation results.

**Acknowledgements**

We acknowledge contributions from science teams of the 12 aircraft campaigns. This work is funded by NOAA Atmospheric Chemistry Carbon Cycle and Climate NA18OAR4310108, NASA Aura Science Team NNX17AH47G, NASA Science of TERRA, AQUA, and SUOMI NPP 80NSSC18K0691, and NASA Making Earth System Data Records for Use in Research Environments 80NSSC18M0091 grants. This work is supported by Center for Computional Science and Engineering at Southern University of Science and Technology. LZ thanks supports from the Smithsonian Astrophysical Observatory (SAO) Visiting Scientist Fellowship. The 2018 WE-CAN campaign was supported by the National Science Foundation (Grant NSF AGS- 1650275, -1650786, -1650288, -1650493, -1652688). LH and WP would like to acknowledge operational, technical and scientific support provided by NCAR's Earth Observing Laboratory, sponsored by the National Science Foundation. This material is based upon work supported by the National Center for Atmospheric Research, which is a major facility sponsored by the National Science Foundation under Cooperative Agreement No. 1852977. The NASA Goddard Space Flight Center (GSFC) team acknowledges support for the ATom campaign from the NASA Earth Venture Suborbital-2 Program, and support for DC3 and SEAC$^4$RS campaigns from NASA.

**References**

Apel, E. C., Hills, A. J., Lueb, R., Zindel, S., Eisele, S., and Riemer, D. D.: A Fast-GC/MS system to measure $C_2$ to $C_4$ carbonyls, and methanol aboard aircraft, J. Geophys. Res., 108, 8794, doi:10.1029/2002JD003199, 2003.

Apel, E. C., Emmons, L. K., Karl, T., Flocke, F., Hills, A. J., Madronich, S., Lee-Taylor, J., Fried, A., Weibring, P., Walega, J., Richter, D., Tie, X., Mauldin, L., Campos, T., Weinheimer, A., Knapp, D., Sive, B., Kleinman, L., Springston, S., Zaveri, R., Ortega, J., Voss, P., Blake, D., Baker, A., Warneke, C., Welsh-Bon, D., de Gouw, J., Zheng, J., Zhang, R., Rudolph, J., Junkermann, W., and Riemer, D. D.: Chemical evolution of volatile organic compounds in the outflow of the Mexico City Metropolitan area, Atmos. Chem. Phys., 10, 2353–2375, https://doi.org/10.5194/acp-10-2353-2010, 2010.

Apel, E. C., Hornbrook, R. S., Hills, A. J., Blake, N. J., Barth, M. C., Weinheimer, A., Cantrell, C., Rutledge, S. A., Basarab, B., Crawford, J., Diskin, G., Homeyer, C. R., Campos, T., Flocke, F., Fried, A., Blake, D. R., Brune, W., Pollack, I., Peischl, J., Ryer- son, T., Wennberg, P. O., Crounse, J. D., Wisthaler, A., Mikoviny, T., Huey, G., Heikes, B.,

O'Sullivan, D., and Riemer, D. D.: Upper tropospheric ozone production from lightning $NO_x$-impacted convection: Smoke ingestion case study from the DC3 campaign,J. Geophys. Res.-Atmos., 120, 2505–2523, 2015.

Barkley, M. P., De Smedt, I., Van Roozendael, M., Kurosu, T. P., Chance, K., Arneth, A., Hagberg, D., Guenther, A., Paulot, F., Marais, E., and Mao, J.: Top-down isoprene emissions over tropical South America inferred from SCIAMACHY and OMI formaldehyde columns, J. Geophys. Res. Atmos., 118, 6849–6868, 2013.

Barth, M. C., Cantrell, C. A., Brune, W. H., Rutledge, S. A., Crawford, J. H., Huntrieser, H., Carey, L. D., MacGorman, D., Weisman, M., Pickering, K. E., Bruning, E., Anderson, B., Apel, E., Biggerstaff, M., Campos, T., Campuzano-Jost, P., Cohen, R., Crounse, J., Day, D. A., Diskin, G., Flocke, F., Fried, A., Garland, C., Heikes, B., Honomichl, S., Hornbrook, R., Huey, L. G., Jimenez, J. L., Lang, T., Lichtenstern, M., Mikoviny, T., Nault, B., O'Sullivan, D., Pan, L. L., Peischl, J., Pollack, I., Richter, D., Riemer, D., Ryerson, T., Schlager, H., St Clair, J., Walega, J., Weibring, P., Weinheimer, A., Wennberg, P., Wisthaler, A., Wooldridge, P. J., and Ziegler, C.: The Deep Convective Clouds and Chemistry (DC3) Field Campaign, B. Am. Meteorol. Soc., 96, 1281–1309, https://doi.org/10.1175/Bams-D-13-00290.1, 2015.

Cao, H., Fu, T.-M., Zhang, L., Henze, D. K., Miller, C. C., Lerot, C., Abad, G. G., De Smedt, I., Zhang, Q., van Roozendael, M., Hendrick, F., Chance, K., Li, J., Zheng, J., and Zhao, Y.: Adjoint inversion of Chinese non-methane volatile organic compound emissions using space-based observations of formaldehyde and glyoxal, Atmos. Chem. Phys., 18, 15017–15046, https://doi.org/10.5194/acp-18-15017-2018, 2018.

Cazorla, M., Wolfe, G. M., Bailey, S. A., Swanson, A. K., Arkinson, H. L., and Hanisco, T. F.: A new airborne laser-induced fluorescence instrument for in situ detection of formaldehyde throughout the troposphere and lower stratosphere, Atmos. Meas. Tech., 8, 541–552, doi:10.5194/amt-8-541-2015, 2015.

Chan Miller, C., Jacob, D. J., Marais, E. A., Yu, K., Travis, K. R., Kim, P. S., Fisher, J. A., Zhu, L., Wolfe, G. M., Hanisco, T. F., Keutsch, F. N., Kaiser, J., Min, K.-E., Brown, S. S., Washenfelder, R. A., González Abad, G., and Chance, K.: Glyoxal yield from isoprene oxidation and relation to formaldehyde: chemical mechanism, constraints from SENEX aircraft observations, and interpretation of OMI satellite data, Atmos. Chem. Phys., 17, 8725–8738, https://doi.org/10.5194/acp-17-8725-2017, 2017.

Chance, K., Palmer, P. I., Spurr, R. J. D., Martin, R. V., Kurosu, T. P., and Jacob, D. J.: Satellite observations of formaldehyde over North America from GOME, Geophys. Res. Lett., 27, 3461–3464, 2000.

Chance, K., and Kurucz, R. L.: An improved high-resolution solar reference spectrum for Earth's atmosphere measurements in the ultraviolet, visible, and near infrared, J. Quant. Spectrosc. Radiat. Transf., 111 (9), 1289–1295, 10.1016/j.jqsrt.2010.01.036, 2010.

Courrèges-Lacoste, G. B., Sallusti, M., Bulsa, G., Bagnasco, G., Veihelmann, B., Riedl, S., Smith, D. J., and Maurer, R.: The Copernicus Sentinel 4 mission: a geostationary imaging UVN spectrometer for air quality monitoring, Proceedings Volume 10423, Sensors, Systems, and Next-Generation Satellites XXI; 1042307, https://doi.org/10.1117/12.2282158, 2017.

Crawford, J. H., and Pickering, K. E.: DISCOVER-AQ Advancing Strategies for Air Quality Observations in the Next Decade, Environ. Manage, 4–7, 2014.

De Smedt, I., Müller, J.-F., Stavrakou, T., van der A, R., Eskes, H., and Van Roozendael, M.: Twelve years of global observations of formaldehyde in the troposphere using GOME and SCIAMACHY sensors, Atmos. Chem. Phys., 8, 4947–4963, doi:10.5194/acp-8-4947-2008, 2008.

De Smedt, I., Van Roozendael, M., Stavrakou, T., Müller, J.-F., Lerot, C., Theys, N., Valks, P., Hao, N., and van der A, R.: Improved retrieval of global tropospheric formaldehyde columns from GOME-2/MetOp-A addressing noise reduction and instrumental degradation issues, Atmos. Meas. Tech., 5, 2933–2949, doi:10.5194/amt-5-2933-2012, 2012.

De Smedt, I., Stavrakou, T., Hendrick, F., Danckaert, T., Vlemmix, T., Pinardi, G., Theys, N., Lerot, C., Gielen, C., Vigouroux, C., Hermans, C., Fayt, C., Veefkind, P., Müller, J.-F., and Van Roozendael, M.: Diurnal, seasonal and long-term variations of global formaldehyde columns inferred from combined OMI and GOME-2 observations, Atmos. Chem. Phys., 15, 12519–12545, doi:10.5194/acp-15-12519-2015, 2015.

De Smedt, I., Theys, N., Yu, H., Danckaert, T., Lerot, C., Compernolle, S., Van Roozendael, M., Richter, A., Hilboll, A., Peters, E., Pedergnana, M., Loyola, D., Beirle, S., Wagner, T., Eskes, H., van Geffen, J., Boersma, K. F., and Veefkind, P.: Algorithm theoretical baseline for formaldehyde retrievals from S5P TROPOMI and from the QA4ECV project, Atmos. Meas. Tech., 11, 2395–2426, https://doi.org/10.5194/amt-11-2395-2018, 2018.

DISCOVER-AQ Science Team: DISCOVER-AQ P-3B Aircraft In-situ Trace Gas Measurements. NASA Langley Atmospheric Science Data Center DAAC, DOI: 10.5067/Aircraft/DISCOVER-AQ/Aerosol-TraceGas, 2014.

Emmons, L.: Merged Data Files containing all C-130 1 Second Observations. Version 1.0. UCAR/NCAR - Earth Observing Laboratory. https://data.eol.ucar.edu/dataset/373.045 (last access: Jul. 10, 2019), 2016.

EPA: National Emissions Inventory, version 2 Technical Support Document, 2015, https://www.epa.gov/sites/production/files/2015-10/documents/nei2011v2_tsd_14aug2015.pdf (last access: Jul. 9, 2019), 2011.

Fried, A., Cantrell, C., Olson, J., Crawford, J. H., Weibring, P., Walega, J., Richter, D., Junkermann, W., Volkamer, R., Sinreich, R., Heikes, B. G., O'Sullivan, D., Blake, D. R., Blake, N., Meinardi, S., Apel, E., Weinheimer, A., Knapp, D., Perring, A., Cohen, R. C., Fuelberg, H., Shetter, R. E., Hall, S. R., Ullmann, K., Brune, W. H., Mao, J., Ren, X., Huey, L. G., Singh, H. B., Hair, J. W., Riemer, D., Diskin, G., and Sachse, G.: Detailed comparisons of airborne formaldehyde measurements with box models during the 2006 INTEX-B and MILAGRO campaigns: potential evidence for significant impacts of unmeasured and multi-generation volatile organic carbon compounds, Atmos. Chem. Phys., 11, 11867–11894, https://doi.org/10.5194/acp-11-11867-2011, 2011.

Giglio, L., Randerson, J. T., and van der Werf, G. R.: Analysis of daily, monthly, and annual burned area using the fourth-geneartion global fire emissions database (GFED4), J. Geophys. Res. Biogeosci., 118, 317–328, doi:10.1002/jgrg.20042, 2013.

González Abad, G., Liu, X., Chance, K., Wang, H., Kurosu, T. P., and Suleiman, R.: Updated Smithsonian Astrophysical Observatory Ozone Monitoring Instrument (SAO OMI) formaldehyde retrieval, Atmos. Meas. Tech., 8, 19–32, https://doi.org/10.5194/amt-8-19-2015, 2015.

González Abad, G., Vasilkov, A., Seftor, C., Liu, X., and Chance, K.: Smithsonian Astrophysical Observatory Ozone Mapping and Profiler Suite (SAO OMPS) formaldehyde retrieval, Atmos. Meas. Tech., 9, 2797–2812, doi:10.5194/amt-9-2797-2016, 2016.

Guenther, A. B., Jiang, X., Heald, C. L., Sakulyanontvittaya, T., Duhl, T., Emmons, L. K., and Wang, X.: The Model of Emissions of Gases and Aerosols from Nature version 2.1 (MEGAN2.1): an extended and updated framework for modeling biogenic emissions, Geosci. Model Dev., 5, 1471–1492, doi:10.5194/gmd-5-1471-2012, 2012.

Herman, J., Spinei, E., Fried, A., Kim, J., Kim, J., Kim, W., Cede, A., Abuhassan, N., and Segal-Rozenhaimer, M.: $NO_2$ and HCHO measurements in Korea from 2012 to 2016 from Pandora spectrometer instruments compared with OMI retrievals and with aircraft measurements during the KORUS-AQ campaign, Atmos. Meas. Tech., 11, 4583–4603, https://doi.org/10.5194/amt-11-4583-2018, 2018.

Hewson,W., Barkley, M. P., González Abad, G., Bösch, H., Kurosu, T., and Spurr, R.: Development and characterisation of a stateof-the-art GOME-2 formaldehyde air-mass factor algorithm, Atmos. Meas. Tech., 8, 4055–4074, doi:10.5194/amt-8-4055-2015, 2015.

Holtslag, A. and Boville, B.: Local versus nonlocal boundary-layer diffusion in a global climate model, J. Clim., 6, 1825–1842, 1993.

Hu, L., and Permar, W.: PTR-ToF-MS Measurements of NMVOCs, HONO, HCN, $CH_3CN$ Data. Version 1.0. UCAR/NCAR - Earth Observing Laboratory. https://doi.org/10.26023/K9F4-2CNH-EQ0W (last access: Nov. 26, 2019), 2019.

Hu, L., Millet, D. B., Baasandorj, M., Griffis, T. J., Turner, P., Helmig, D., Curtis, A. J., and Hueber, J.: Isoprene emissions and impacts over an ecological transition region in the US Upper Midwest inferred from tall tower measurements, J. Geophys. Res.-Atmos., 120, 3553–3571, 2015.

Jaeglé, L., Thornton, J. A., Brown, S. S., Shah, V., Lopez-Hilfiker, F., Lee, B. H., Haskins, J., Fibiger, D. L., McDuffie, E. E., Sparks, T., Ebben, C. J., Wooldridge, P. J., Cohen, R. C., Veres, P. R., Weinheimer, A. J., Montzka, D. D., Dibb, J. E., Schroder, J. C., Jost, P. C., Day, D. A., Jimenez, J. L., Sullivan, A., Guo, H., Weber, R. J., Green, J. R., Fiddler, M. N., Bililign, S., Campos, T. L., Apel E. C., Blake, N. J., Hall, S. R., Ullmann, K., Wolfe, G. M., DiGangi, J. P., Hanisco, T. F., Leen, J. B.: Sources, Chemistry, and Transport of Pollutants over the Eastern United States During the WINTER 2015 Aircraft Campaign, AGU Fall Meeting, 2015.

Jin, X. and Holloway, T.: Spatial and temporal variability of ozone sensitivity over China observed from the Ozone Monitoring Instrument, J. Geophys. Res.-Atmos., 120, 7229–7246, https://doi.org/10.1002/2015JD023250, 2015.

Jin, X., Fiore, A. M., Murray, L. T., Valin, L. C., Lamsal, L. N., Duncan, B., Folkert Boersma, K., De Smedt, I., Abad, G. G., Chance, K., and Tonnesen, G. S.: Evaluating a space-based indicator of surface ozone-$NO_x$-VOC sensitivity over midlatitude source regions and application to decadal trends, J. Geophys. Res.-Atmos., 122, 439–461, https://doi.org/10.1002/2017JD026720, 2017.

Khokhar, M., Frankenberg, C., Roozendael, M. V., Beirle, S., Kuhl, S., Richter, A., Platt, U., and Wagner, T.: Satellite observations of atmospheric $SO_2$ from volcanic eruptions during the time-period of 1996–2002, Adv. Space Res., 36, 879–887, doi:10.1016/j.asr.2005.04.114, 2005.

Kim, J., Jeong, U., Ahn, M., Kim, J. H., Park, R. J., Lee, H., Song, C. H., Choi, Y., Lee, K., Yoo, J., Jeong, M., Park, S. K., Lee, K., Song, C., Kim, S., Kim, Y., Kim, S., Kim, M., Go, S., Liu, X., Chance, K., Chan Miller, C., Al-Saadi, J., Veihelmann, B., Bhartia, P. K., Torres, O., González Abad, G., Haffner, D. P., Ko, D. H., Lee, S. H., Woo, J., Chong, H., Park, S. S., Nicks, D., Choi, W. J., Moon, K., Cho, A., Yoon, J., Kim, S., Hong, H., Lee, K., Lee, H., Lee, S., Choi, M., Veefkind, P., Levelt, P., Edwards, D. P., Kang, M., Eo, M., Bak, J., Baek, K., Kwon, H., Yang, J., Park, J., Han, K. M., Kim, B., Shin, H., Choi, H., Lee, E., Chong, J., Cha, Y., Koo, J., Irie, H., Hayashida, S., Kasai, Y., Kanaya, Y., Liu, C., Lin, J., Crawford, J. H., Carmichael, G. R., Newchurch, M. J., Lefer, B. L., Herman, J. R., Swap, R. J., Lau, A. K., Kurosu, T. P., Jaross, G., Ahlers, B., Dobber, M., McElroy, C. and Choi, Y.: New Era of Air Quality Monitoring from Space: Geostationary Environment Monitoring Spectrometer (GEMS). Bull. Amer. Meteor. Soc., https://doi.org/10.1175/BAMS-D-18-0013.1, 2019.

Kleipool, Q. L., Dobber, M. R., de Haan, J. F., and Levelt, P. F.: Earth surface reflectance climatology from 3 years of OMI data, J. Geophys. Res.-Atmos., 113, D18308, doi:10.1029/2008JD010290, 2008.

KORUS-AQ: An International Cooperative Air Quality Field Study in Korea, available at: https://www-air.larc.nasa.gov/missions/korus-aq/ (last access: Oct. 22, 2019), DOI: 10.5067/Suborbital/KORUSAQ/DATA01, 2016.

Kwon, H.-A., Park, R. J., Jeong, J. I., Lee, S., González Abad, G., Kurosu, T. P., Palmer, P. I., and Chance, K.: Sensitivity of formaldehyde (HCHO) column measurements from a geostationary satellite to temporal variation of the air mass factor in East Asia, Atmos. Chem. Phys., 17, 4673–4686, https://doi.org/10.5194/acp-17-4673-2017, 2017.

Kwon, H.-A., Park, R. J., González Abad, G., Chance, K., Kurosu, T. P., Kim, J., De Smedt, I., Van Roozendael, M., Peters, E., and Burrows, J.: Description of a formaldehyde retrieval algorithm for the Geostationary Environment Monitoring Spectrometer (GEMS), Atmos. Meas. Tech., 12, 3551–3571, https://doi.org/10.5194/amt-12-3551-2019, 2019.

Li, C., Joiner, J., Krotkov, N. A., and Dunlap, L.: A newmethod for global retrievals of HCHO total columns from the Suomi National Polar-orbiting Partnership Ozone Mapping and Profiler Suite, Geophys. Res. Lett., 42, 2515–2522, 2015.

Li, M., Zhang, Q., Kurokawa, J.-I., Woo, J.-H., He, K., Lu, Z., Ohara, T., Song, Y., Streets, D. G., Carmichael, G. R., Cheng, Y., Hong, C., Huo, H., Jiang, X., Kang, S., Liu, F., Su, H., and Zheng, B.: MIX: a mosaic Asian anthropogenic emission inventory under the international collaboration framework of the MICS-Asia and HTAP, Atmos. Chem. Phys., 17, 935 963, https://doi.org/10.5194/acp-17-935-2017, 2017.

Liao, J., Hanisco, T. F., Wolfe, G. M., St. Clair, J., Jimenez, J. L., Campuzano-Jost, P., Nault, B. A., Fried, A., Marais, E. A., González Abad, G., Chance, K., Jethva, H. T., Ryerson, T. B., Warneke, C., and Wisthaler, A.: Towards a satellite formaldehyde – in situ hybrid estimate for organic aerosol abundance, Atmos. Chem. Phys., 19, 2765–2785, https://doi.org/10.5194/acp-19-2765-2019, 2019.

Lin, J.-T. and McElroy, M.: Impacts of boundary layer mixing on pollutant vertical profiles in the lower troposphere: Implications to satellite remote sensing, Atmos. Environ., 44, 1726–1739, 2010.

Marais, E. A., Jacob, D. J., Kurosu, T. P., Chance, K., Murphy, J. G., Reeves, C., Mills, G., Casadio, S., Millet, D. B., Barkley, M. P., Paulot, F., and Mao, J.: Isoprene emissions in Africa inferred from OMI observations of formaldehyde columns, Atmos. Chem. Phys., 12, 6219–6235, doi:10.5194/acp-12-6219-2012, 2012.

Martin, R. V., Parrish, D. D., Ryerson, T. B., Nicks Jr., D. K., Chance, K., Kurosu, T. P., Jacob, D. J., Sturges, E. D., Fried, A., and Wert, B. P.: Evaluation of GOME satellite measurements of tropospheric $NO_2$ and HCHO using regional data from aircraft campaigns in the southeastern United States, J. Geophys. Res.-Atmos., 109, D24307, doi:10.1029/2004JD004869, 2004.

Millet, D. B., Baasandorj, M., Farmer, D. K., Thornton, J. A., Baumann, K., Brophy, P., Chaliyakunnel, S., de Gouw, J. A., Graus, M., Hu, L., Koss, A., Lee, B. H., Lopez- Hilfiker, F. D., Neuman, J. A., Paulot, F., Peischl, J., Pollack, I. B., Ryerson, T. B., Warneke, C., Williams, B. J., and Xu, J.: A large and ubiquitous source of atmospheric formic acid, Atmos. Chem. Phys., 15, 6283–6304, doi:10.5194/acp-15-6283-2015, 2015.

Molod, A., Takacs, L., Suarez, M., Bacmeister, J., Song, I.-S., and Eichmann, A.: The GEOS-5 Atmospheric General Circulation Model: Mean Climate and Development from MERRA to Fortuna, NASA/TM–2012, 104606, 28, 1–124, 2012.

Müller, M., Mikoviny, T., Feil, S., Haidacher, S., Hanel, G., Hartungen, E., Jordan, A., Märk, L., Mutschlechner, P., Schottkowsky, R., Sulzer, P., Crawford, J. H., and Wisthaler, A.: A compact PTR-ToF-MS instrument for airborne measurements of volatile organic compounds at high spatiotemporal resolution, Atmos. Meas. Tech., 7, 3763–3772, https://doi.org/10.5194/amt-7-3763-2014, 2014.

National Oceanic and Atmospheric Administration (NOAA): SONGNEX 2015 CSD Data Archive, Earth System Research Laboratory, Chemical Sciences Division, available at: https://www.esrl.noaa.gov/csd/projects/songnex/ (last access: Oct. 22, 2019), 2017.

Nowlan, C. R., Liu, X., Janz, S. J., Kowalewski, M. G., Chance, K., Follette-Cook, M. B., Fried, A., González Abad, G., Herman, J. R., Judd, L. M., Kwon, H.-A., Loughner, C. P., Pickering, K. E., Richter, D., Spinei, E., Walega, J., Weibring, P., and Weinheimer, A. J.: Nitrogen dioxide and formaldehyde measurements from the GEOstationary Coastal and Air Pollution Events (GEO-CAPE) Airborne Simulator over Houston, Texas, Atmos. Meas. Tech., 11, 5941–5964, https://doi.org/10.5194/amt-11-5941-2018, 2018.

Palmer, P. I., Jacob, D. J., Chance, K., Martin, R. V., Spurr, R. J. D., Kurosu, T. P., Bey, I., Yantosca, R., Fiore, A., and Li, Q.: Air mass factor formulation for spectroscopic measurements from satellites: Application to formaldehyde retrievals from the Global Ozone Monitoring Experiment, J. Geophys. Res.-Atmos., 106, 14539–14550, 2001.

Palmer, P. I., Jacob, D. J., Fiore, A. M., Martin, R. V., Chance, K., and Kurosu, T. P.: Mapping isoprene emissions over North America using formaldehyde column observations from space, J. Geophys. Res.-Atmos., 108, 4180, doi:10.1029/2002JD002153, 2003.

Pfister, G., Flocke, F., Hornbrook, R., Orlando, J., Lee, S., Schroeder, J., and NASA Langley Research Center: Process-Based and Regional Source Impact Analysis for FRAPPÉ and DISCOVER-AQ 2014, available at: https://www.colorado.gov/airquality/tech_doc_repository.aspx?action=open&file=FRAPPE-NCAR_Final_Report_July2017.pdf (last access: Nov. 02, 2019), 2017.

Pollack, I. B., Lindaas, J., Roscioli, J. R., Agnese, M., Permar, W., Hu, L., and Fischer, E. V.: Evaluation of ambient ammonia measurements from a research aircraft using a closed-path QC-TILDAS operated with active continuous passivation, Atmos. Meas. Tech., 12, 3717–3742, https://doi.org/10.5194/amt-12-3717-2019, 2019.

Richter, D., Weibring, P., Walega, J. G., Fried, A., Spuler, S. M., and Taubman, M. S.: Compact highly sensitive multi-species airborne mid-IR spectrometer, Appl. Phys. B, 119, 119–131, 2015.

Scarino, A. J., Obland, M. D., Fast, J. D., Burton, S. P., Ferrare, R. A., Hostetler, C. A., Berg, L. K., Lefer, B., Haman, C., Hair, J. W., Rogers, R. R., Butler, C., Cook, A. L., and Harper, D. B.: Comparison of mixed layer heights from airborne high spectral resolution lidar, ground-based measurements, and the WRF-Chem model during CalNex and CARES, Atmos. Chem. Phys., 14, 5547–5560, doi:10.5194/acp-14-5547-2014, 2014.

Schenkeveld, V. M. E., Jaross, G., Marchenko, S., Haffner, D., Kleipool, Q. L., Rozemeijer, N. C., Veefkind, J. P., and Levelt, P. F.: In-flight performance of the Ozone Monitoring Instrument, Atmos. Meas. Tech., 10, 1957–1986, https://doi.org/10.5194/amt-10-1957-2017, 2017.

Shim, C., Wang, Y., Choi, Y., Palmer, P. I., Abbot, D. S., and Chance, K.: Constraining global isoprene emissions with Global Ozone Monitoring Experiment (GOME) formaldehyde column measurements, J. Geophys. Res.-Atmos., 110, D24301, doi:10.1029/2004JD005629, 2005.

Stavrakou, T., Müller, J.-F., De Smedt, I., Van Roozendael, M., van der Werf, G. R., Giglio, L., and Guenther, A.: Global emissions of non-methane hydrocarbons deduced from SCIAMACHY formaldehyde columns through 2003–2006, Atmos. Chem. Phys., 9, 3663–3679, doi:10.5194/acp-9-3663-2009, 2009.

Singh, H. B., Brune, W. H., Crawford, J. H., Flocke, F., and Jacob, D. J.: Chemistry and transport of pollution over the Gulf of Mexico and the Pacific: spring 2006 INTEX-B campaign overview and first results, Atmos. Chem. Phys., 9, 2301–2318, doi:10.5194/acp-9-2301-2009, 2009.

Surl, L., Palmer, P. I., and González Abad, G.: Which processes drive observed variations of HCHO columns over India?, Atmos. Chem. Phys., 18, 4549-4566, https://doi.org/10.5194/acp-18-4549-2018, 2018.

Tan, W., Liu, C., Wang, S., Xing, C., Su, W., Zhang, C., Xia, C., Liu, H., Cai, Z., and Liu, J.: Tropospheric $NO_2$, $SO_2$, and HCHO over the East China Sea, using ship-based MAX-DOAS observations and comparison with OMI and OMPS satellite data, Atmos. Chem. Phys., 18, 15387–15402, https://doi.org/10.5194/acp-18-15387-2018, 2018.

Toon, O. B., Maring, H., Dibb, J., Ferrare, R., Jacob, D. J., Jensen, E. J., Luo, Z. J., Mace, G. G., Pan, L. L., Pfister, L., Rosenlof, K. H., Redemann, J., Reid, J. S., Singh, H. B., Thompson, A. M., Yokelson, R., Minnis, P., Chen, G., Jucks, K. W., and Pszenny, A.: Planning, implementation, and scientific goals of the Studies of Emissions and Atmospheric Composition, Clouds and Climate Coupling by Regional Surveys (SEAC$^4$RS) field mission, J. Geophys. Res.-Atmos., 121, 4967–5009, https://doi.org/10.1002/2015jd024297, 2016.

UCAR/NCAR - Earth Observing Laboratory, Jaegle, L., Shah, V.: 1s Merged dataset of all C-130 observations and GEOS-Chem near-realtime simulations for WINTER. Version 1.1. UCAR/NCAR - Earth Observing Laboratory. https://doi.org/10.5065/D68C9TDX (last access: Jul. 10, 2019), 2016.

Vigouroux, C., Hendrick, F., Stavrakou, T., Dils, B., De Smedt, I., Hermans, C., Merlaud, A., Scolas, F., Senten, C., Vanhaelewyn, G., Fally, S., Carleer, M., Metzger, J.-M., Müller, J.-F., Van Roozendael, M., and De Mazière, M.: Ground-based FTIR and MAX-DOAS observations of formaldehyde at Réunion Island and comparisons with satellite and model data, Atmos. Chem. Phys., 9, 9523–9544, doi:10.5194/acp-9-9523-2009, 2009.

Wang, Y., Beirle, S., Lampel, J., Koukouli, M., De Smedt, I., Theys, N., Li, A., Wu, D., Xie, P., Liu, C., Van Roozendael, M., Stavrakou, T., Müller, J.-F., and Wagner, T.: Validation of OMI, GOME-2A and GOME-2B tropospheric $NO_2$, $SO_2$ and HCHO products using MAX-DOAS observations from 2011 to 2014 in Wuxi, China: investigation of the effects of priori profiles and aerosols on the satellite products, Atmos. Chem. Phys., 17, 5007–5033, https://doi.org/10.5194/acp-17-5007-2017, 2017.

Wang, Y., Wang, Z., Yu, C., Zhu, S., Cheng, L., Zhang, Y., and Chen, L.: Validation of OMI HCHO Products Using MAX-DOAS observations from 2010 to 2016 in Xianghe, Beijing: Investigation of the Effects of Aerosols on Satellite Products, Remote Sens., 11(2), 203, https://doi.org/10.3390/rs11020203, 2019.

Warneke, C., Trainer, M., de Gouw, J. A., Parrish, D. D., Fahey, D. W., Ravishankara, A. R., Middlebrook, A. M., Brock, C. A., Roberts, J. M., Brown, S. S., Neuman, J. A., Lerner, B. M., Lack, D., Law, D., Hübler, G., Pollack, I., Sjostedt, S., Ryerson, T. B., Gilman, J. B., Liao, J., Holloway, J., Peischl, J., Nowak, J. B., Aikin, K. C., Min, K.-E., Washenfelder, R. A., Graus, M. G., Richardson, M., Markovic, M. Z., Wagner, N. L., Welti, A., Veres, P. R., Edwards, P., Schwarz, J. P., Gordon, T., Dube, W. P., McKeen, S. A., Brioude, J., Ahmadov, R., Bougiatioti, A., Lin, J. J., Nenes, A., Wolfe, G. M., Hanisco, T. F., Lee, B. H., Lopez-Hilfiker, F. D., Thornton, J. A., Keutsch, F. N., Kaiser, J., Mao, J., and Hatch, C. D.: Instrumentation and measurement strategy for the NOAA SENEX aircraft campaign as part of the Southeast Atmosphere Study 2013, Atmos. Meas. Tech., 9, 3063–3093, https://doi.org/10.5194/amt-9-3063-2016, 2016.

Weibring, P., Richter, D., Fried, A., Walega, J., and Dyroff, C.: Ultra-high-precision mid-IR spectrometer II: system description and spectroscopic performance, Appl. Phys. B, 85, 207–218, https://doi.org/10.1007/s00340-006-2300-4, 2006.

Weibring, P., Richter, D., Walega, J. G., and Fried, A.: First demonstration of a high performance difference frequency spectrometer on airborne platforms, Opt. Express, 15, 13476–13495, https://doi.org/10.1364/OE.15.013476, 2007.

Weibring, P., Richter, D., Walega, J. G., Rippe, L., and Fried, A.: Difference frequency generation spectrometer for simultaneous multispecies detection., Opt. Express, 18(26), 27670–27681, doi:10.1364/OE.18.027670, 2010.

Wittrock, F., Richter, A., Oetjen, H., Burrows, J. P., Kanakidou, M., Myriokefalitakis, S., Volkamer, R., Beirle, S., Platt, U., and Wagner, T.: Simultaneous global observations of glyoxal and formaldehyde from space, Geophys. Res. Lett., 33, L16804, doi:10.1029/2006GL026310, 2006.

Wofsy, S. C., Afshar, S., Allen, H. M., Apel, E., Asher, E. C., Bar- letta, B., Bent, J., Bian, H., Biggs, B. C., Blake, D. R., Blake, N., Bourgeois, I., Brock, C. A., Brune, W. H., Budney, J. W., Bui, T. P., Butler, A., Campuzano-Jost, P., Chang, C. S., Chin, M., Commane, R., Correa, G., Crounse, J. D., Cullis, P. D., Daube, B. C., Day, D. A., Dean-Day, J. M., Dibb, J. E., DiGangi, J. P., Diskin, G. S., Dollner, M., Elkins, J. W., Erdesz, F., Fiore, A. M., Flynn, C. M., Froyd, K., Gesler, D. W., Hall, S. R., Hanisco, T. F., Hannun, R. A., Hills, A. J., Hintsa, E. J., Hoffman, A., Hornbrook, R. S., Huey, L. G., Hughes, S., Jimenez, J. L., Johnson, B. J., Katich, J. M., Keeling, R. F., Kim, M. J., Kupc, A., Lait, L. R., Lamarque, J.-F., Liu, J., McKain, K., Mclaughlin, R. J., Meinardi, S., Miller, D. O., Montzka, S. A., Moore, F. L., Morgan, E. J., Murphy, D. M., Murray, L. T., Nault, B. A., Neuman, J. A., Newman, P. A., Nicely, J. M., Pan, X., Paplawsky, W., Peischl, J., Prather, M. J., Price, D. J., Ray, E., Reeves, J. M., Richardson, M., Rollins, A. W., Rosenlof,

K. H., Ryerson, T. B., Scheuer, E., Schill, G. P., Schroder, J. C., Schwarz, J. P., St.Clair, J. M., Steenrod, S. D., Stephens, B. B., Strode, S. A., Sweeney, C., Tanner, D., Teng, A. P., Thames, A. B., Thompson, C. R., Ullmann, K., Veres, P. R., Vieznor, N., Wagner, N. L., Watt, A., Weber, R., Weinzierl, B., Wennberg, P., Williamson, C. J., Wilson, J. C., Wolfe, G. M., Woods, C. T., and Zeng, L. H.: ATom: Merged Atmospheric Chemistry, Trace Gases, and Aerosols. ORNL DAAC, Oak Ridge, Ten- nessee, USA, https://doi.org/10.3334/ornldaac/1581, 2018.

Wolfe, G. M., Nicely, J. M., St. Clair, J. M., Hanisco, T. F., Liao, J., Oman, L. D., Brune, W. B., Miller, D., Thames, A., González Abad, G., Ryerson, T. B., Thompson, C. R., Peischl, J., McKain, K., Sweeney, C., Wennberg, P. O., Kim, M., Crounse, J. D., Hall, S. R., Ullmann, K., Diskin, G., Bui, P., Chang, C., and Dean-Day, J.: Mapping hydroxyl variability throughout the global remote troposphere via synthesis of airborne and satellite formaldehyde observations, PNAS, 116 (23) 11171-11180, https://doi.org/10.1073/pnas.1821661116, 2019.

Zhu, L., Jacob, D. J., Mickley, L. J., Marais, E. A., Cohan, D. S., Yoshida, Y., Duncan, B. N., González Abad, G., and Chance, K. V.: Anthropogenic emissions of highly reactive volatile organic compounds in eastern Texas inferred from oversampling of satellite (OMI) measurements of HCHO columns, Environ. Res. Lett., 9, 114004, doi:10.1088/1748-9326/9/11/114004, 2014.

Zhu, L., Jacob, D. J., Kim, P. S., Fisher, J. A., Yu, K., Travis, K. R., Mickley, L. J., Yantosca, R. M., Sulprizio, M. P., De Smedt, I., González Abad, G., Chance, K., Li, C., Ferrare, R., Fried, A., Hair, J. W., Hanisco, T. F., Richter, D., Jo Scarino, A., Walega, J., Weibring, P., and Wolfe, G. M.: Observing atmospheric formaldehyde (HCHO) from space: validation and intercomparison of six retrievals from four satellites (OMI, GOME2A, GOME2B, OMPS) with SEAC$^4$RS aircraft observations over the southeast US, Atmos. Chem. Phys., 16, 13477–13490, https://doi.org/10.5194/acp-16-13477-2016, 2016.

Zhu, L., Mickley, L. J., Jacob, D. J., Marais, E. A., Sheng, J., Hu, L., González Abad, G., and Chance, K.: Long-term (2005–2014) trends in formaldehyde (HCHO) columns across North America as seen by the OMI satellite instrument: Evidence of changing emissions of volatile organic compounds, Geophys. Res. Lett., 44, 7079–7086, https://doi.org/10.1002/2017GL073859, 2017a.

Zhu, L., Jacob, D. J., Keutsch, F. N., Mickley, L. J., Scheffe, R., Strum, M., Abad, G. G., Chance, K., Yang, K., Rappengluck, B., Millet, D. B., Baasandorj, M., Jaegle, L., and Shah, V.: Formaldehyde (HCHO) As a Hazardous Air Pollutant: Mapping Surface Air Concentrations from Satellite and Inferring Cancer Risks in the United States, Environ. Sci. Technol., 51, 5650–5657, https://doi.org/10.1021/acs.est.7b01356, 2017b.

Zoogman, P., Liu, X., Suleiman, R. M., Pennington, W. F., Flittner, D. E., Al-Saadi, J. A., Hilton, B. B., Nicks, D. K., Newchurch, M. J., Carr, J. L., Janz, S. J., Andraschko, M. R., Arola, A., Baker, B. D., Canova, B. P., Chan Miller, C., Cohen, R. C., Davis, J. E., Dussault, M. E., Edwards, D. P., Fishman, J., Ghulam, A., González Abad, G., Grutter, M., Herman, J. R., Houck, J., Jacob, D. J., Joiner, J., Kerridge, B. J., Kim, J., Krotkov, N. A., Lamsal, L., Li, C., Lindfors, A., Martin, R. V., McElroy, C. T., McLin- den, C., Natraj, V., Neil, D. O., Nowlan, C. R., OSullivan, E. J., Palmer, P. I., Pierce, R. B., Pippin, M. R., Saiz-Lopez, A., Spurr, R. J. D., Szykman, J. J., Torres, O., Veefkind, J. P., Veihelmann, B., Wang, H., Wang, J., and Chance, K.: Tropospheric emissions: Monitoring of pollution (TEMPO), J. Quant. Spectrosc. Ra., 186, 17–39, doi:10.1016/j.jqsrt.2016.05.008, 2017.

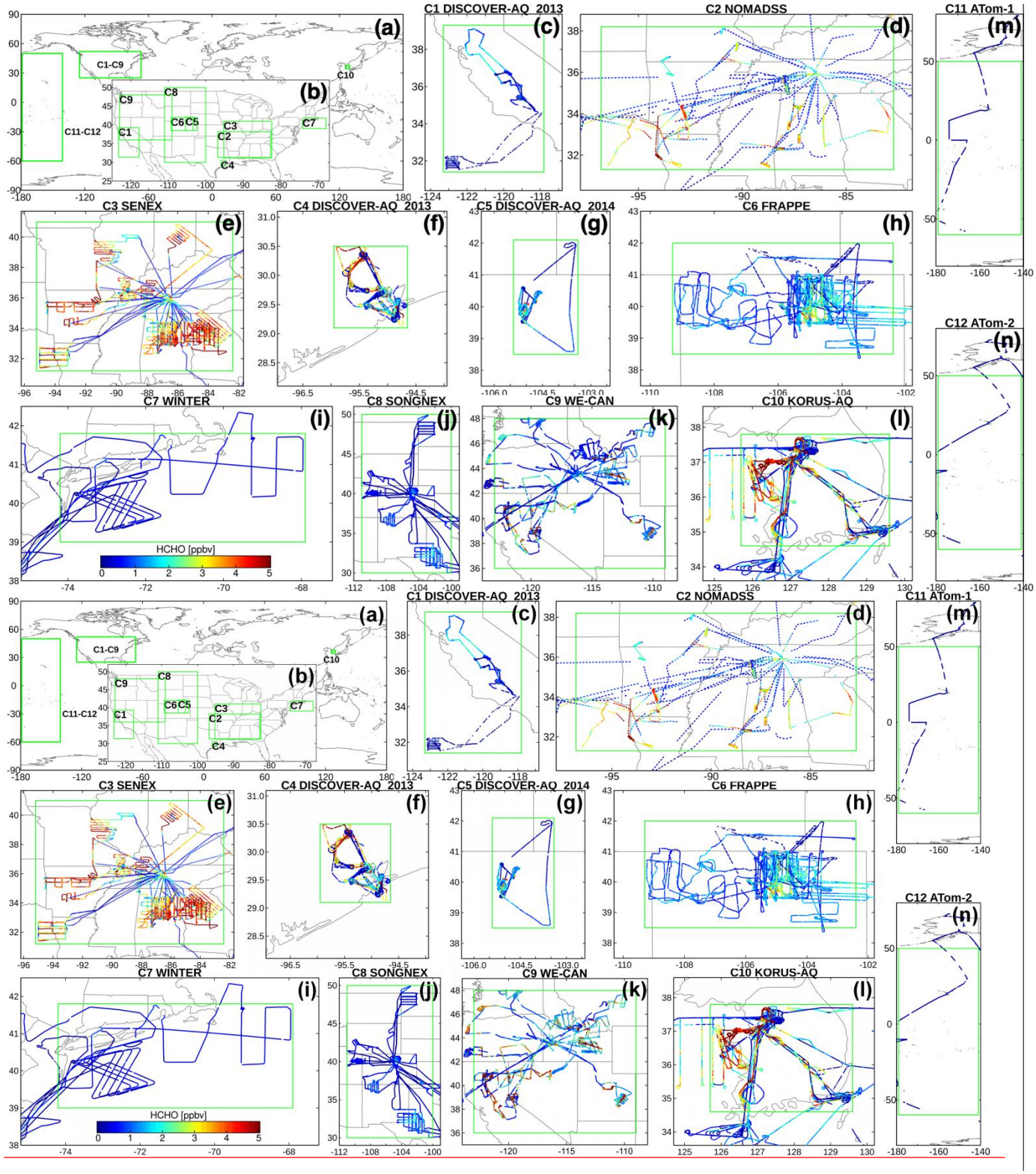
(a)
C1-C9
C10
C11-C12
(b)
C9
C8
C6 C5
C3
C2
C1
C7
C4
C1 DISCOVER-AQ 2013
(c)
C2 NOMADSS
(d)
C11 ATom-1
(m)
C3 SENEX
(e)
C4 DISCOVER-AQ 2013
(f)
C5 DISCOVER-AQ 2014
(g)
C6 FRAPPE
(h)
C12 ATom-2
(n)
C7 WINTER
(i)
HCHO [ppbv]
0 1 2 3 4 5
C8 SONGNEX
(j)
C9 WE-CAN
(k)
C10 KORUS-AQ
(l)

**Figure 1.** Flight tracks of the 12 aircraft campaigns used in this study. Panel (a) shows the spatial coverage (green rectangles) of the campaigns. Panel (b) (inset) zooms in campaigns over the United States. Aircraft campaigns are numbered as C1–C12. Table 1 summarizes detailed information of the 12 campaigns. Formaldehyde (HCHO) mixing ratios along aircraft flight tracks are shown in panel (c)–(n). Color bar saturates at 5 ppbV. The green rectangle in panel (c)–(n) is the same as that in (a) and (b), indicating spatial domain of a certain campaign. The same domain is also defined in Table 1.

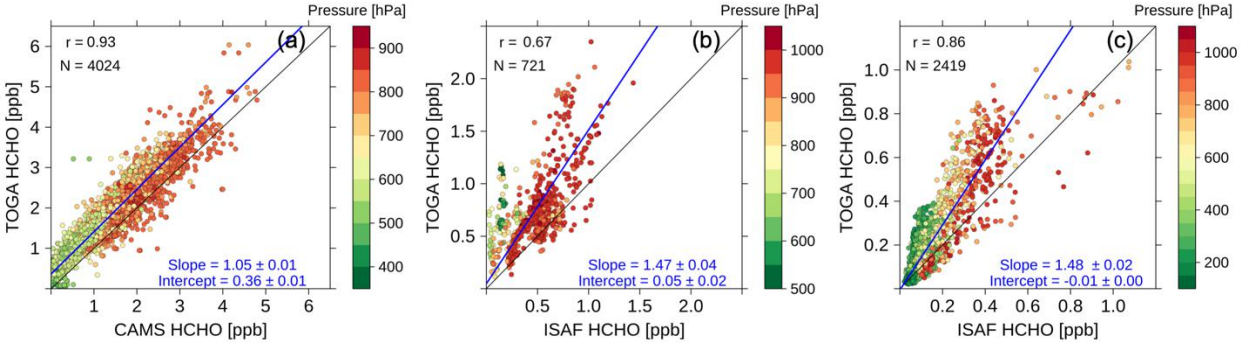


**Figure 2.** Comparisons between 1-min averaged HCHO observations from multiple instruments. (a) Observations from TOGA and CAMS instruments aboard the NSF/NCAR C-130 during the FRAPPÉ campaign. (b) Observations from TOGA and ISAF instruments aboard the NSF/NCAR C-130 during the WINTER campaign. (c) Observations from TOGA and ISAF instruments aboard the NASA DC-8 during the ATom-2 campaign. HCHO data points are colored by atmospheric pressure. Reduced major axis (RMA) regression slops and intercepts are shown along with the correlation coefficient (*r*), sample size (*N*), RMA regression line (blue) and 1:1 line (black).

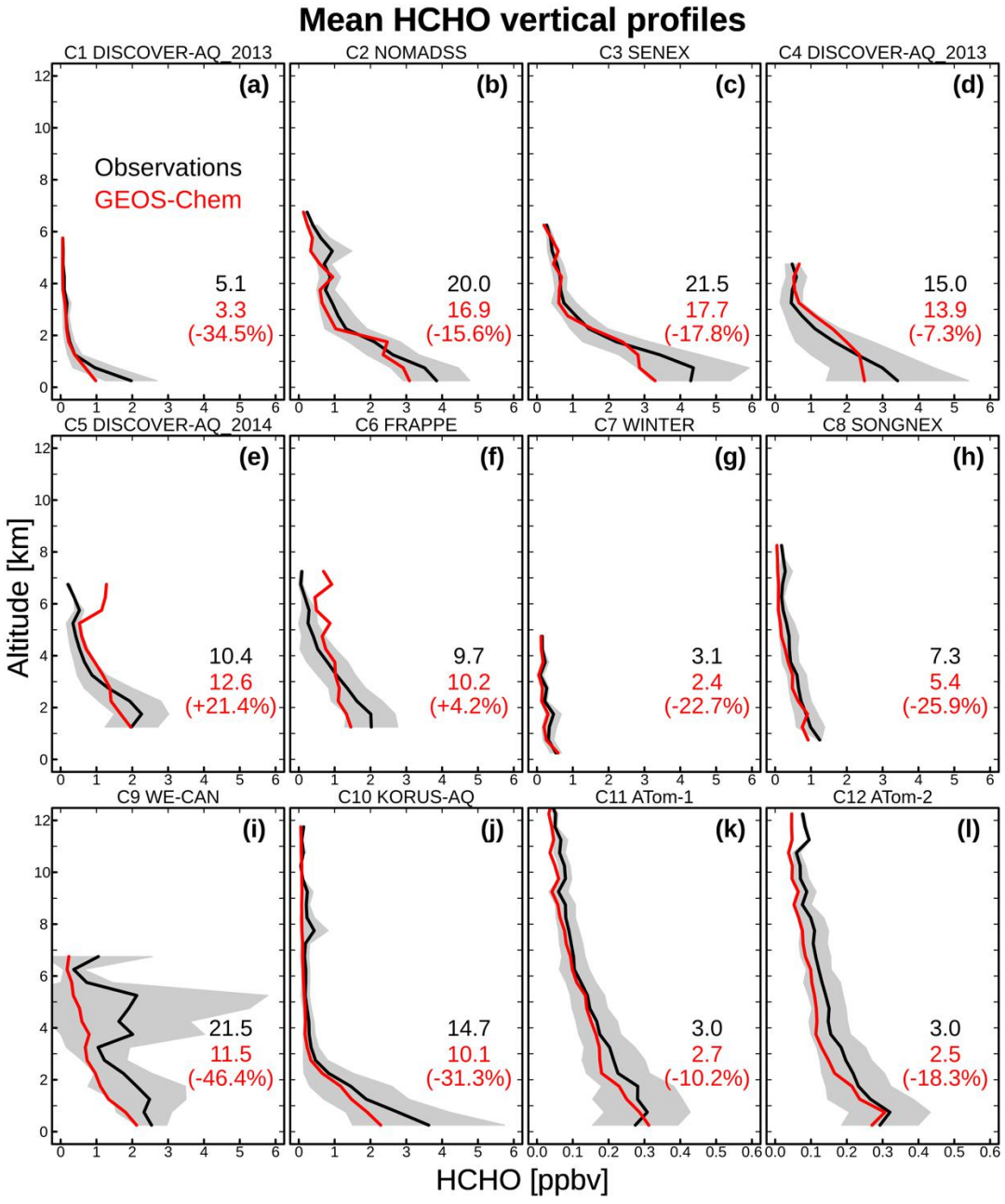
Mean HCHO vertical profiles
C1 DISCOVER-AQ_2013
C2 NOMADSS
C3 SENEX
C4 DISCOVER-AQ_2013
C5 DISCOVER-AQ_2014
C6 FRAPPE
C7 WINTER
C8 SONGNEX
C9 WE-CAN
C10 KORUS-AQ
C11 ATom-1
C12 ATom-2
(a)
(b)
(c)
(d)
(e)
(f)
(g)
(h)
(i)
(j)
(k)
(l)
Observations
GEOS-Chem
5.1
3.3
(-34.5%)
20.0
16.9
(-15.6%)
21.5
17.7
(-17.8%)
15.0
13.9
(-7.3%)
10.4
12.6
(+21.4%)
9.7
10.2
(+4.2%)
3.1
2.4
(-22.7%)
7.3
5.4
(-25.9%)
21.5
11.5
(-46.4%)
14.7
10.1
(-31.3%)
3.0
2.7
(-10.2%)
3.0
2.5
(-18.3%)
Altitude [km]
HCHO [ppbv]

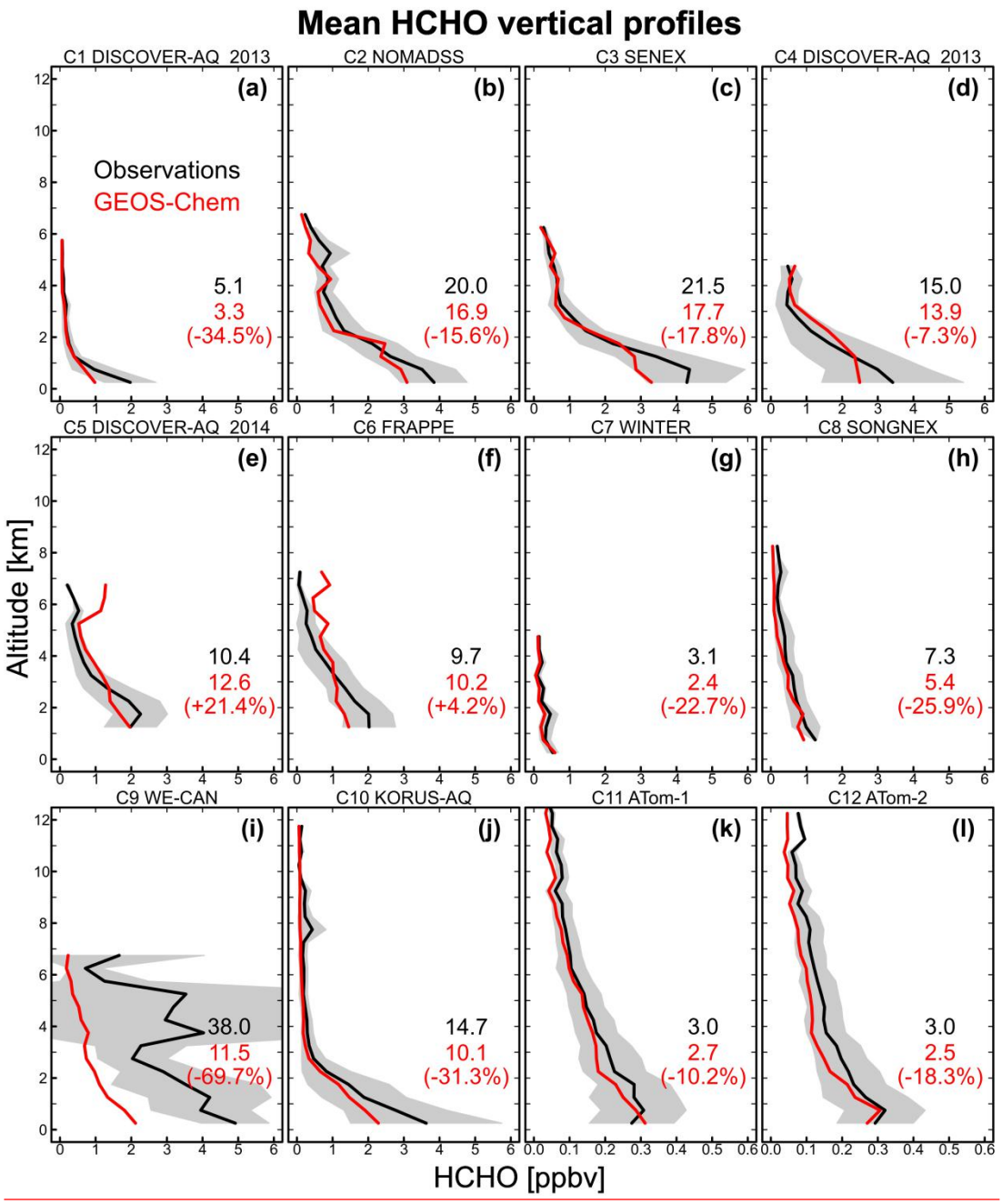


685

**Figure 3.** Mean HCHO vertical profiles as observed during the 12 aircraft campaigns (Table 1) and simulated by GEOS-Chem. GEOS-Chem is sampled along the flight tracks at the time and locations of the measurements. We only use observed and modeled HCHO values within the study area, defined by the green rectangle for each campaign in Figure 1. HCHO values are vertically binned in increments of 500 m. Shading gives the standard deviation in the observations. Observed (black) and modeled (red) HCHO column densities ($10^{15}$ molecules $cm^{-2}$) are insert along with relative biases (in parentheses) in modeled column densities. The relative biases are further used as correction factors for GOES-Chem columns. Observed column densities are computed using mean observed mixing ratio (black lines), temperature, and pressure. Modeled column densities are computed according to GEOS-Chem HCHO vertical profiles (red lines) as well as temperature and pressure from GEOS-FP. Notice that scale in panel (k) and (l) is different from that in other panels.

690

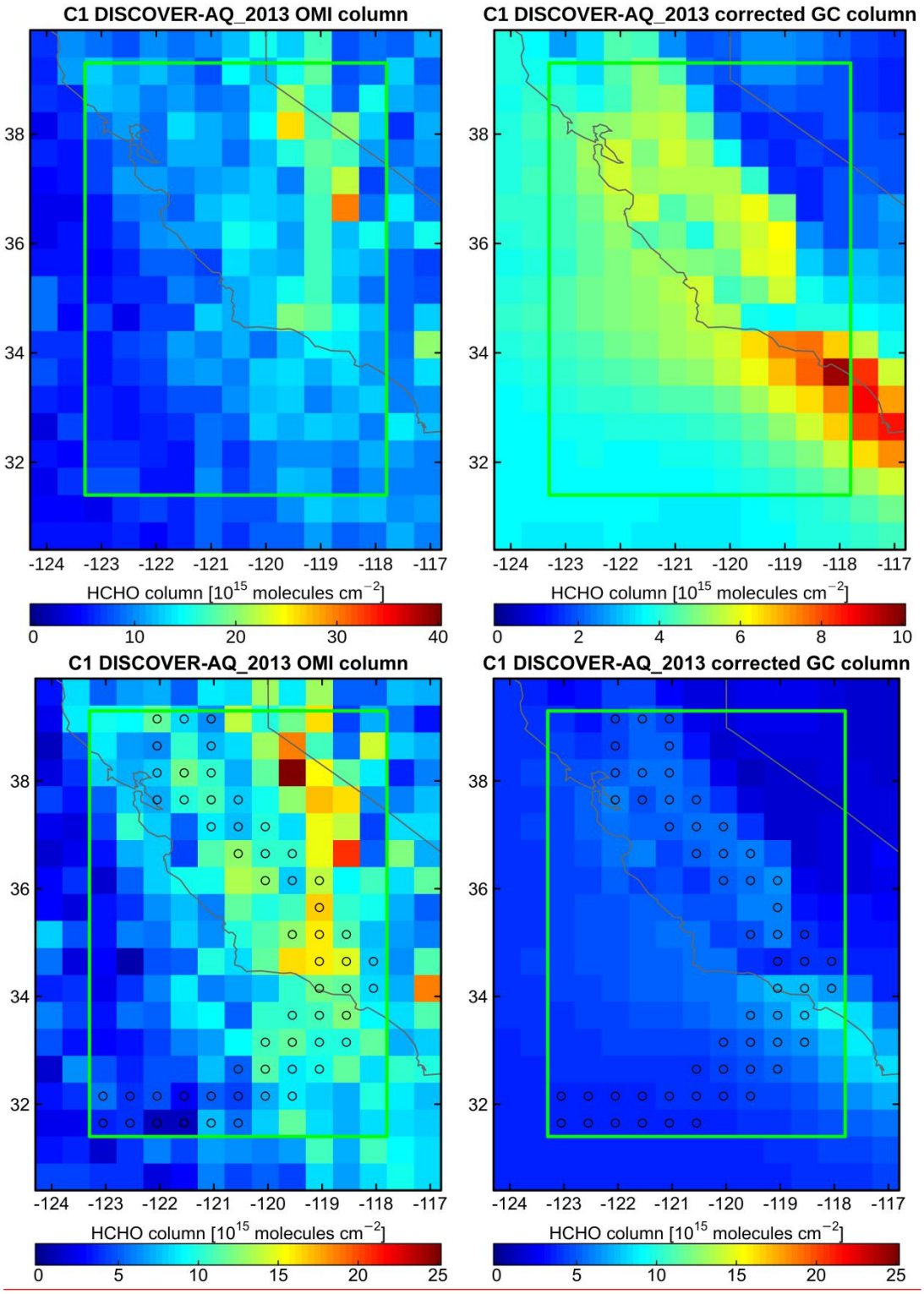
C1 DISCOVER-AQ_2013 OMI column
C1 DISCOVER-AQ_2013 corrected GC column
38
36
34
32
-124 -123 -122 -121 -120 -119 -118 -117
HCHO column [10^15 molecules cm^-2]
0 10 20 30 40
0 2 4 6 8 10
C1 DISCOVER-AQ_2013 OMI column
C1 DISCOVER-AQ_2013 corrected GC column
HCHO column [10^15 molecules cm^-2]
0 5 10 15 20 25

695

**Figure 4.** HCHO vertical column densities over California, United States during the DISCOVER-AQ California 2013 (C1; 16 Jan. – 6 Feb.). The left panel shows data from OMI SAO HCHO product. The right panel shows GEOS-Chem model results sampled on the OMI schedule (see text), and scaled by a factor of 1.53 to correct for the bias relative to aircraft measurements (Figure 3). OMI and GEOS-Chem results are regridded onto the 0.5°×0.5° grids. The green rectangles represent the study domain (same as that in Figure 1), which is also defined in Table 1. ~~Notice~~ Here and elsewhere, validation results (*e.g.*, in Table 2) are limited to the ~~two panels~~ grids marked with black open circles, which represent grids that are sampled by the aircraft (*i.e.*, intercepted with flight tracks in ~~different HCHO scales~~Figure 1). .

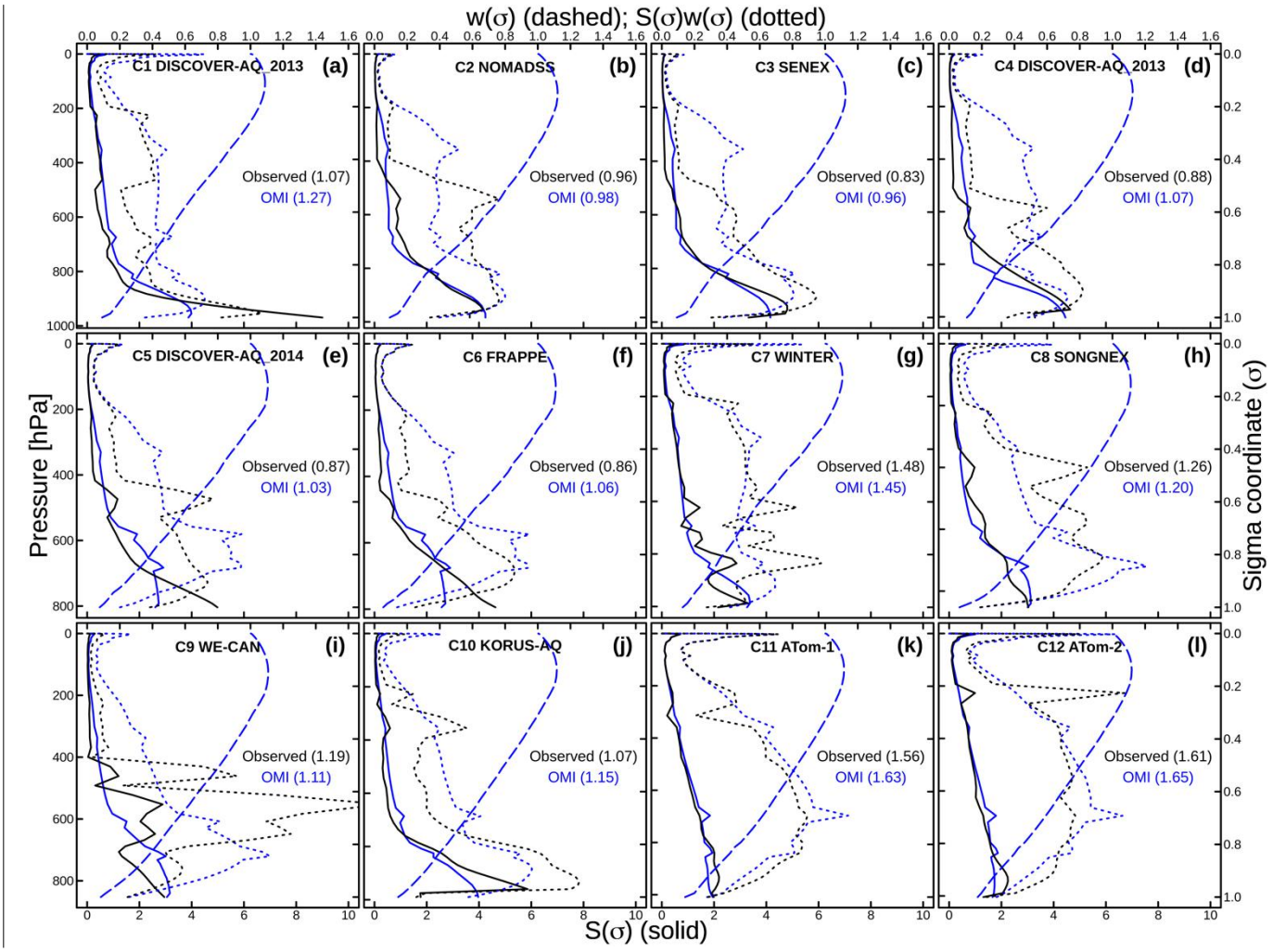
w(σ) (dashed); S(σ)w(σ) (dotted)
C1 DISCOVER-AQ, 2013
(a)
Observed (1.07)
OMI (1.27)
C2 NOMADSS
(b)
Observed (0.96)
OMI (0.98)
C3 SENEX
(c)
Observed (0.83)
OMI (0.96)
C4 DISCOVER-AQ, 2013
(d)
Observed (0.88)
OMI (1.07)
C5 DISCOVER-AQ, 2014
(e)
Observed (0.87)
OMI (1.03)
C6 FRAPPE
(f)
Observed (0.86)
OMI (1.06)
C7 WINTER
(g)
Observed (1.48)
OMI (1.45)
C8 SONGNEX
(h)
Observed (1.26)
OMI (1.20)
C9 WE-CAN
(i)
Observed (1.19)
OMI (1.11)
C10 KORUS-AQ
(j)
Observed (1.07)
OMI (1.15)
C11 ATom-1
(k)
Observed (1.56)
OMI (1.63)
C12 ATom-2
(l)
Observed (1.61)
OMI (1.65)
Pressure [hPa]
Sigma coordinate (σ)
S(σ) (solid)

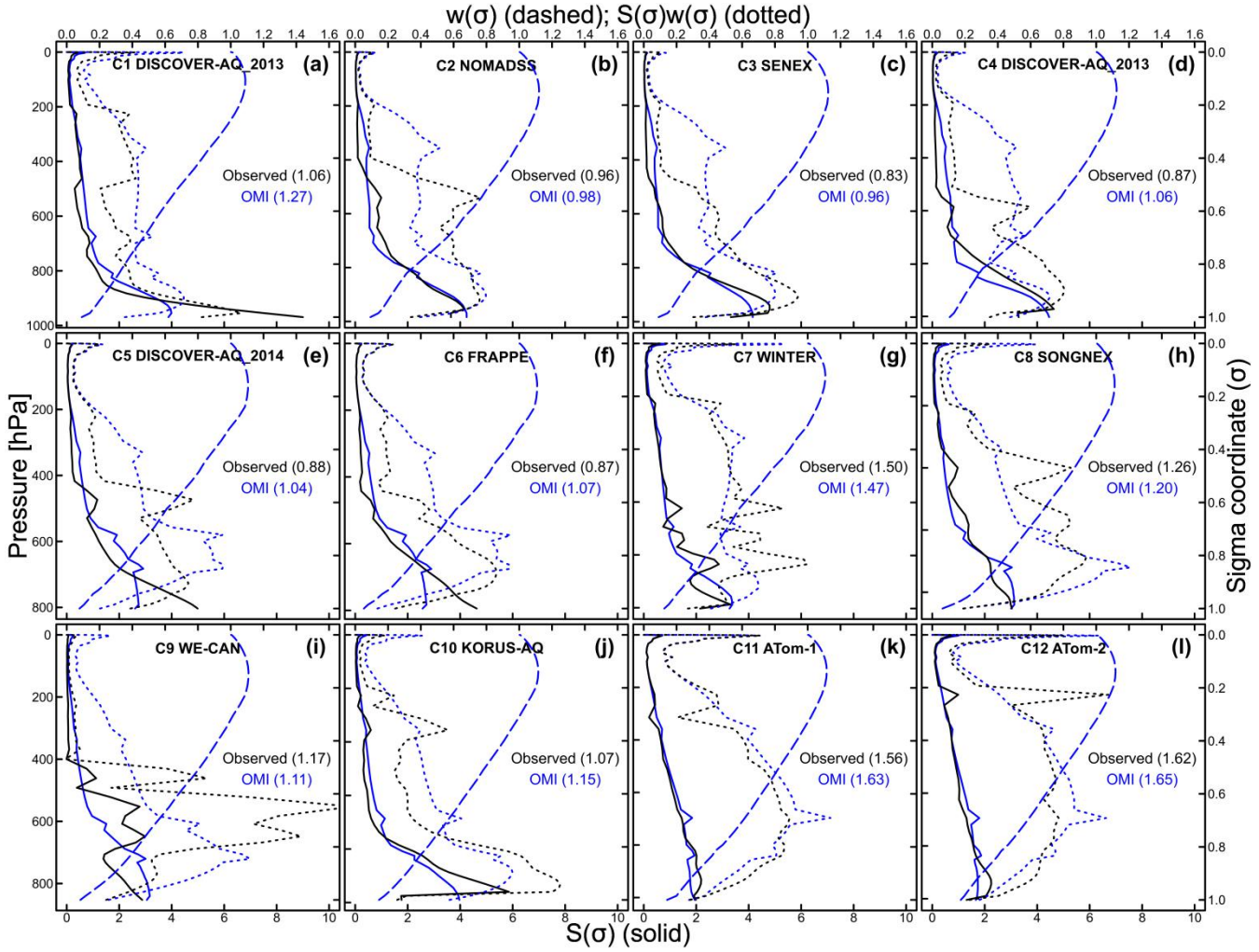


**Figure 5.** Air mass factor (AMF) components over the 12 aircraft campaigns. Each panel shows mean scattering weights (*w*; blue dashed line) and shape factors (*S*; blue solid line) from OMI SAO HCHO product averaged over the corresponding ~~study domain (shown~~ grids sampled by the aircrafts (marked with open circles in Figure ~~1; defined in Table 1~~4 and S1-S11) during the campaign period (defined in Table 1), as well as the product of the two (blue dotted line) from which mean AMF is derived by vertical integration using equation (4). Each panel also shows observed HCHO shape factors (black solid) from the mean HCHO profile in Figure 3. We use mean HCHO profiles from ATom-1 and ATom-2 (Figure 3) to fill observations above 6 km. Also shown is the product (black dotted line) of mean OMI scattering weights (blue dashed line) and observed HCHO shape factor (black solid). Mean AMF values are given in the legend computed using OMI (blue) and observed (black) shape factors.

**Table 1.** Overview of the 12 aircraft campaigns used in this study

| Campaign ID | Campaign name | Region | Date | Platform | HCHO instrument(s) [a] | Domain [b] | References [c] |
|---|---|---|---|---|---|---|---|
| C1 | DISCOVER-AQ California 2013 | California, U.S. | Jan. 16–Feb. 06 2013 | NASA P-3B | DFGAS (4%) | 31.4–39.3N 123.3–117.8W | 1, 2 |
| C2 | NOMADSS | Southeastern U.S. | Jun. 03–Jul. 14 2013 | NSF/NCAR C130 | TOGA (15%) [d] | 31.3–38.2N 96.8–82.7W | 3 |
| C3 | SENEX | Southeastern U.S. | Jun. 03–Jul. 10 2013 | NOAA WP-3D | ISAF (10%) | 31.2–41.0N 95.2–82.4W | 4 |
| C4 | DISCOVER-AQ Texas 2013 | Texas, U.S. | Sep. 04–Sep. 29 2013 | NASA P-3B | DFGAS (4%) | 29.1–30.5N 95.95–94.65W | 1, 2 |
| C5 | DISCOVER-AQ Colorado 2014 | Colorado, U.S. | Jul. 17–Aug. 10 2014 | NASA P-3B | DFGAS (4%) | 38.5–42.1N 105.4–103.4W | 1, 2 |
| C6 | FRAPPÉ | Colorado, U.S. | Jul. 26–Aug. 18 2014 | NSF/NCAR C130 | CAMS (4%) TOGA (15%) [d] | 38.5–42.0N 109.3–102.4W | 5, 6 |
| C7 | WINTER | Northeastern U.S. | Feb. 03–Mar. 13 2015 | NSF/NCAR C-130 | ISAF (10%) TOGA (15%) [d] | 39.0–41.8N 72.2–67.9W | 7 |
| C8 | SONGNEX | Western U.S. | Mar. 19–Apr. 27 2015 | NOAA WP-3D | ISAF (10%) | 30.0–50.0N 111.0–100.0W | 8 |
| C9 | WE-CAN | Western U.S. | Jul. 26–Sep. 13 2018 | NSF/NCAR C-130 | PTR-ToF-MS (60%) | 36.0–48.0N 123.0–109.0W | 9, 10 |
| C10 | KORUS-AQ | South Korea | Apr. 26–Jun. 18 2016 | NASA DC-8 | CAMS (4%) | 34.6–37.8N 125.7–129.6W | 11 |
| C11 | ATom-1 | Pacific Ocean | Jul. 29–Aug. 23 2016 | NASA DC-8 | ISAF (10%) | 60.0S–50N 179.0–141.0W | 12 |
| C12 | ATom-2 | Pacific Ocean | Jan. 26–Feb. 21 2017 | NASA DC-8 | ISAF (10%) TOGA (15%) [d] | 60.0S–50N 179.0–141.0W | 12 |

[a] Instrument accuracy is given in parentheses. During C6, C7, and C12, HCHO is measured by two independent instruments

[b] Shown as green rectangles in Figure 1

[c] 1 Crawford and Pickering [2014]; 2 DISCOVER-AQ Science Team [2014]; 3 Emmons [2016]; 4 Warneke et al. [2016]; 5 Pfister et al. [2017]; 6 Richter et al. [2015]; 7 UCAR/NCAR - Earth Observing Laboratory et al. [2016]; 8 National Oceanic and Atmospheric Administration (NOAA) [2017]; 9 Pollack et al. [2019]; 10 Hu and Permar [2019]; 11 KORUS-AQ [2016]; 12 Wofsy et al. [2018]

[d] TOGA has an accuracy of 15% or better

720 **Table 2.** HCHO columns and validation results over the 12 aircraft campaigns [a]

| Campaign ID | GEOS-Chem columns | | | OMI | | | | | with observed shape factors | |
|---|---|---|---|---|---|---|---|---|---|---|
| | Original [b] | Corrected [c] | $AMF_G$ | AMF | $\Omega_S$ [d] | $\Omega_{S0}$ [e] | $\Omega_{avg}$ [f] | $\Omega_{comp}$ [g] | AMF [h] | $\Omega_{comp}$ [i] |
| C1 | 2.82 | 4.30 | 3.14 | 1.25 | 16.40 | 5.03 | 10.25 (+138.4%) | 9.07 (+110.9%) | 1.07 | 10.66 (+148.0%) |
| C2 | 15.49 | 18.36 | 2.54 | 0.97 | 16.78 | 4.73 | 13.24 (–27.9%) | 12.42 (–32.4%) | 0.96 | 12.58 (–31.5%) |
| C3 | 14.53 | 17.68 | 2.48 | 0.95 | 16.87 | 4.53 | 13.88 (–21.5%) | 12.95 (–26.8%) | 0.83 | 14.85 (–16.0%) |
| C4 | 16.05 | 17.32 | 2.68 | 1.07 | 17.45 | 5.10 | 11.97 (–30.90%) | 11.52 (–33.5%) | 0.88 | 14.06 (–18.8%) |
| C5 | 6.13 | 5.05 | 2.49 | 1.02 | 15.88 | 3.85 | 13.58 (+168.7%) | 11.85 (+134.6%) | 0.87 | 13.89 (+174.8%) |
| C6 [j] | 5.59 | 5.37 | 2.54 | 1.05 | 15.47 | 4.02 | 12.44 (+131.6%) | 10.90 (+102.9%) | 0.86 | 13.30 (+147.7%) |
| C7 [k] | 2.66 | 3.44 | 3.19 | 1.45 | 12.09 | 1.23 | 8.79 (+155.6%) | 7.49 (+117.8%) | 1.48 | 7.33 (+113.1%) |
| C8 | 2.75 | 3.71 | 2.59 | 1.19 | 15.19 | 3.27 | 10.92 (+194.6%) | 10.02 (+170.4%) | 1.26 | 9.47 (+155.5%) |
| C9 | 5.85 | 10.92 | 2.60 | 1.09 | 16.11 | 3.57 | 12.67 (+16.0%) | 11.49 (+5.2%) | 1.19 | 10.55 (–3.5%) |
| C10 | 7.34 | 10.69 | 2.59 | 1.15 | 16.36 | 5.14 | 10.49 (–1.8%) | 9.79 (–8.4%) | 1.07 | 10.45 (–2.3%) |
| C11 | 2.66 | 2.97 | 2.75 | 1.61 | 11.86 | 1.56 | 6.72 (+126.6%) | 6.39 (+115.4%) | 1.56 | 6.60 (+122.5%) |
| C12 [k] | 2.61 | 3.19 | 2.78 | 1.64 | 12.06 | 1.52 | 6.82 (+113.9%) | 6.42 (+101.4%) | 1.61 | 6.53 (+104.8%) |
| SEAC[4]RS [l] | 15.23 | 16.90 | 2.66 | 0.95 | - | - | 10.60 (–37.0%) | - | - | - |
| | Original [b] | Corrected [c] | $r$ [d] | $AMF_G$ | AMF | $\Omega_S$ [e] | $\Omega_{S0}$ [f] | $\Omega_{avg}$ [g] | $\Omega_{comp}$ [h] | AMF [i] | $\Omega_{comp}$ [j] |
| C1 | 2.86 | 4.37 | -0.08 | 3.14 | 1.21 | 14.13 | 4.90 | 8.90 (+103.9%) | 7.63 (+74.7%) | 1.06 | 8.67 (+98.7%) |
| C2 | 15.47 | 18.33 | -0.17 | 2.54 | 0.97 | 15.41 | 4.89 | 11.59 (–36.8%) | 10.85 (–40.8%) | 0.96 | 10.97 (–40.1%) |

| | | | | | | | | | | | |
|---|---|---|---|---|---|---|---|---|---|---|---|
| C3 | 14.88 | 18.11 | -0.05 | 2.49 | 0.93 | 15.57 | 4.57 | 12.66 (–30.1%) | 11.86 (–34.5%) | 0.83 | 13.26 (–26.8%) |
| C4 | 17.89 | 19.31 | 0.72 | 2.68 | 0.99 | 17.20 | 5.06 | 12.53 (–35.1%) | 12.32 (–36.2%) | 0.87 | 13.91 (–28.0%) |
| C5 | 6.52 | 5.37 | -0.22 | 2.51 | 1.06 | 12.88 | 4.05 | 9.50 (+76.8%) | 8.30 (+54.6%) | 0.88 | 10.08 (+87.6%) |
| C6 [k] | 5.64 | 5.41 | -0.13 | 2.55 | 1.03 | 12.45 | 4.26 | 9.31 (+72.0%) | 7.95 (+46.9%) | 0.87 | 9.47 (+75.0%) |
| C7 [l] | 2.76 | 3.57 | 0.30 | 3.18 | 1.53 | 9.14 | 1.42 | 6.55 (+83.7%) | 5.03 (+41.1%) | 1.50 | 5.14 (+44.0%) |
| C8 | 2.93 | 3.96 | -0.27 | 2.60 | 1.18 | 12.46 | 3.48 | 8.39 (+112.1%) | 7.59 (+91.9%) | 1.26 | 7.12 (+80.0%) |
| C9 | 5.61 | 18.53 | 0.06 | 2.60 | 1.07 | 13.79 | 3.75 | 10.28 (–44.5%) | 9.40 (–49.3%) | 1.17 | 8.57 (–53.7%) |
| C10 | 7.86 | 11.45 | 0.18 | 2.59 | 1.13 | 14.89 | 5.33 | 8.96 (–21.7%) | 8.47 (–26.0%) | 1.07 | 8.93 (–22.0%) |
| C11 | 2.70 | 3.01 | 0.49 | 2.75 | 1.56 | 9.21 | 1.47 | 5.20 (+72.9%) | 4.95 (+64.5%) | 1.56 | 4.96 (+64.8%) |
| C12 [l] | 2.42 | 2.95 | 0.25 | 2.78 | 1.71 | 9.57 | 1.91 | 4.91 (+66.1%) | 4.50 (+52.1%) | 1.62 | 4.75 (+60.7%) |
| SEAC$^4$RS [m] | 15.23 | 16.90 | 0.38 | 2.66 | 0.95 | - | - | 10.60 (–37.0%) | - | - | - |

[a] Results are spatially and temporally averaged values for the ~~study regions (shown as green rectangles~~ grids sampled by the aircrafts (marked with open circles in Figure ~~1~~ 4 and ~~defined in Table 1~~S1-S11) during the study periods (defined in Table 1). HCHO columns (GEOS-Chem columns, $\Omega_S$, $\Omega_{S0}$, $\Omega_{avg}$, and $\Omega_{comp}$) are in the unit of $10^{15}$ molecules cm$^{-2}$. For each aircraft campaign, biases relative to the corrected GEOS-Chem column are given in parentheses

[b] sampled from the GEOS-Chem models according to OMI's schedule

[c] corrected with the factors informed by comparison of observed and modeled HCHO columns (Figure 3)

[d] spatial correlation between GEOS-Chem and OMI HCHO column over the study region (green rectangles in Figure 1)

[e] SCD computed using vertical column density without reference sector correction ("ColumnAmount" data field in OMI SAO HCHO product) and air mass factor (AMF)

[e~~f~~] SCD correction term recomputed using averaged OMI $\Omega_S$, $\Omega_{avg}$, and AMF following equation (1)

[f~~g~~] mean VCD by directly averaging valid satellite pixels

[g~~h~~] VCD recomputed using averaged OMI $\Omega_S$, $\Omega_{S0}$, and AMF following equation (1)

[h~~i~~] recomputed using averaged OMI $AMF_G$, observed mean HCHO shape factors (Figure 5), and mean OMI scattering weights (Figure 5) following equation (3)–(5)

[i~~j~~] VCD computed using recomputed AMF, averaged OMI $\Omega_S$, and averaged OMI $\Omega_{S0}$ following equation (1)–(2)

[j~~k~~] using CAMS observations

[k~~l~~] using ISAF observations

[l~~m~~] results reported by Zhu et al. [2016] over the southeastern United States (30.5–39.0N, 95.0–81.5W) during Aug. 05–Sep. 25, 2013. Results are based on a different version of GEOS-Chem model